Enabling Scalable Direct Air Capture With Concentrated Solar Power

Process Modelling and Techno-Economic Analysis

ME55035
Ruben Gerritse

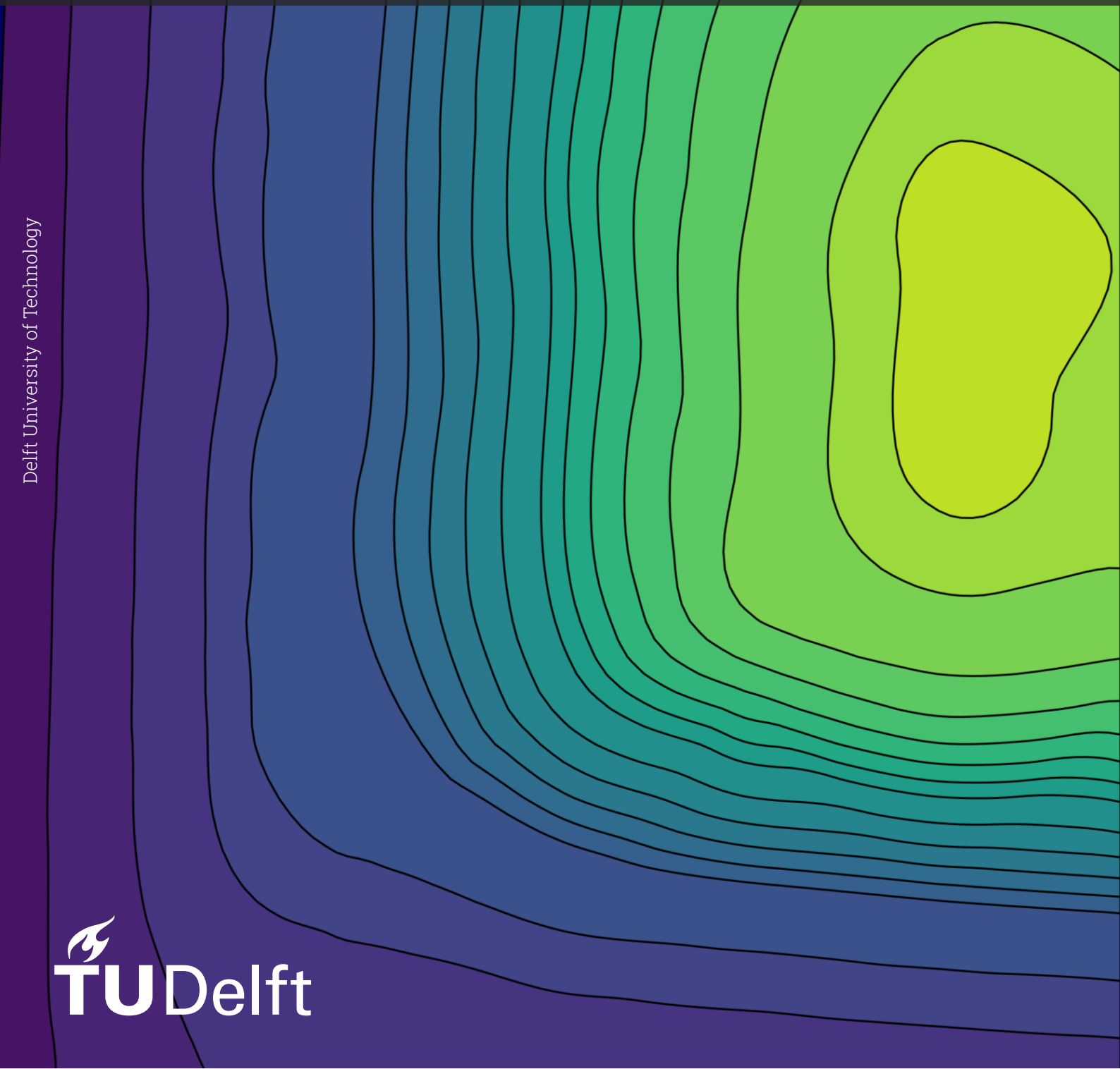

Delft University of Technology

TU Delft

Enabling Scalable Direct Air Capture With Concentrated Solar Power

Process Modelling and Techno-Economic Analysis

by

Ruben Gerritse

to obtain the degree of Master of Science
at the Delft University of Technology,
to be defended publicly on Friday July 25, 2025 at 10:00 AM.

Student number:	4898346	
Project duration:	September 27, 2024 – July 25, 2025	
Thesis committee:	Dr. ir. T.M.J. Nijssen,	TU Delft, supervisor
	Dr. ir. M. Ramadin	TU Delft
	Dr. E. Zanetti	TU Delft

An electronic version of this thesis is available at `http://repository.tudelft.nl/`.

TU Delft

Preface

I always had an interest in sustainable technologies, so diving deeper into direct air capture and concentrated solar power was a topic close to my heart. Exploring how the combination of two systems works, was a fascinating puzzle, especially when things started to come together. It was very rewarding to see how much you get to know of a topic when you spent so many hours, struggling from time to time with grasping the concepts.

I am especially grateful for my supervisor, Tim Nijssen, who gave me a lot of support and insights during the process. He was really invested in the project and it was good to see that he also clearly enjoyed thinking along with me and seeing the results. Besides his insights, support and encouragements, I really enjoyed the small coffee brakes.

I am very thankful that I did not have to work all by myself, and am therefore grateful to all the friends I got to work besides and have breaks with. They made the working days feel shorter and far more enjoyable. Besides the fun chats, it was also interesting to see where they work on and how we could sometimes help each other out. I also greatly appreciate the feedback and sparring with my roommates from time to time.

I am curious to see where life will bring me next, and I look forward to applying all the things I learned in practice, both during my studies and along the way.

Ruben Gerritse
Delft, July 2025

Abstract

This thesis explores the integration of solid sorbent direct air capture (DAC) with two types of concentrated solar power, to create a renewable and scalable approach for carbon dioxide removal. Parabolic trough collector (PTC) and solar power tower (SPT) systems are modelled dynamically on an hourly basis, combined with the energy requirement and performance of the DAC model. Because system output is highly sensitive to climatic conditions, two high-irradiance locations in Almeria, Spain and Alice Springs, Australia are evaluated using typical meteorological year data.

The results show that SPT outperforms PTC in achieving the lowest levelised cost of CO_2 removal (LCOD), primarily due to its lower thermal energy storage costs. The configuration optimised for LCOD involves significant oversizing of the solar field and storage, far larger than the configuration optimised for cost of heat. This increases the capacity, and utilises the CAPEX-intensive DAC installation to a greater extent. These DAC costs are the main cost driver accounting for 68% of the cost for a conservative scenario. A sensitivity analysis reveals that lowering the DAC costs is found not to change the optimal configuration significantly, allowing the LCOD of a lower CAPEX scenario to be determined accurately from the results.

The weather conditions in Alice Springs result in a reduction of the LCOD by up to 27% compared to Almeria, due to higher and more constant solar availability combined with lower humidities. While PTC systems have higher LCOD, they require significantly less land. Overall, the combination of CSP and DAC is technically viable and it offers a scalable, land efficient alternative to nature based carbon dioxide removal methods.

Contents

Preface i

Abstract ii

Nomenclature iv

1 Introduction 1
- 1.1 Research questions . . . 4
- 1.2 Approach . . . 4

2 Methods 5
- 2.1 Physics of Adsorption . . . 5
  - 2.1.1 Sorbent Loading CO_2 . . . 5
  - 2.1.2 Sorbent Loading H_2O . . . 6
  - 2.1.3 Diffusion Limitations . . . 6
  - 2.1.4 Mass Balances . . . 7
  - 2.1.5 Energy Balance . . . 8
  - 2.1.6 System Settings . . . 9
  - 2.1.7 Model Validation . . . 10
- 2.2 Modelling Concentrated Solar Power . . . 12
  - 2.2.1 Physics of Concentrated Solar Power . . . 13
  - 2.2.2 System Control . . . 14
  - 2.2.3 SAM Simulations . . . 14
- 2.3 Energy Requirement DAC . . . 16
  - 2.3.1 Electrical Demand . . . 16
  - 2.3.2 Thermal Energy Demand . . . 16
- 2.4 Cost Calculations . . . 17
  - 2.4.1 Thermal Energy Storage . . . 18

3 Results 20
- 3.1 Sizing CSP . . . 20
- 3.2 Cost Sensitivity Analysis . . . 22
- 3.3 Weather Influence . . . 24
- 3.4 CO_2 Capture per Land Use . . . 26
- 3.5 CSP Validation . . . 27

4 Conclusion 28

5 Recommendations 29

References 30

A Faster adsorption model 34
- A.1 Edge cases . . . 35
  - A.1.1 Inlet edge case . . . 35
  - A.1.2 Outlet edge case . . . 35
  - A.1.3 Validate average assumption . . . 36
  - A.1.4 Model limits . . . 36
- A.2 Faster desorption improvement . . . 37
  - A.2.1 Verification . . . 38

Nomenclature

Abbreviations

CCS	Carbon capture and storage
CDR	Carbon dioxide removal
CO	Cost optimum configuration
CSP	Concentrated solar power
CST	Concentrated solar thermal
DAC	Direct air capture
DNI	Direct normal irradiance [kWh/m^2/year]
HTF	Heat-transfer fluid
HS	Hours of storage
LCOD CO_2	Levelized cost of removed CO_2
LCOP CO_2	Levelized cost of produced CO_2
LCOE	Levelized cost of electricity
L-DAC	Liquid solvent DAC
MA	Minimum area configuration
PTC	Parabolic through collector
PV	Photovoltaic
S-DAC	Solid sorbent DAC
SM	Solar multiple
SPT	Solar power tower
TVSA	Temperature-vacuum swing adsorption

Subscripts

ap	Aperture
CO_2	Carbon-dioxide
c	Collector
g	Gas
H_2O	Water
ht	High temperature
l	Land use
r	Receiver
s	Sorbent
st	Steam

Symbols

Symbol	Definition	Unit
A	Surface area	m^2
a_s	Area per volume	$m^2 \cdot m^{-3}$
b	Equilibrium parameter	Pa^{-1}
C	Water concentration parameter	-
C_p	Specific heat capacity	$J \cdot mol^{-1} \cdot K^{-1}$
c	Concentration	$mol \cdot m^{-3}$
D_{AB}	Molecular diffusion coefficient	-
D_{Kn}	Knudsen diffusion coefficient	-
D_p	Effective pore diffusion coefficient	-
e	Specific energy	$J \cdot kg^{-1}$
E_{act}	Molar activation energy	$J \cdot mol^{-1}$
ΔH	Isosteric heat of adsorption	$J \cdot mol^{-1}$
ΔH_c	Enthalpy of monolayer adsorption	$J \cdot mol^{-1}$
ΔH_k	Enthalpy of multilayer adsorption	$J \cdot mol^{-1}$
$\Delta_r H$	Reaction heat	$J \cdot mol^{-1}$
Δh_{vap}	Heat of vaporisation	$J \cdot kg^{-1}$
h_t	Heat transfer coefficient	$W \cdot m^{-2} \cdot K^{-1}$
K	Water concentration parameter	-
k_T	Reaction rate constant	$mol \cdot kg^{-1} \cdot Pa^{-1} \cdot s^{-1}$
L	Length of bed	m
M	Molar mass	$mol \cdot kg^{-1}$
m_s	Mass of sorbent	kg
p	Partial pressure	Pa
$\dot{Q}$	Flow rate	$m^3 \cdot s^{-1}$
q	Sorbent loading	$mol \cdot kg^{-1}$
q_s	Maximum sorbent loading	$mol \cdot kg^{-1}$
R	Gas constant	$J \cdot mol^{-1} \cdot K^{-1}$
R_a	Intrinsic adsorption rate	$mol \cdot kg^{-1} \cdot s^{-1}$
RH	Relative humidity	-
r_s	Particle radius	m
S	Selectivity	-
T	Temperature	K
t_h	Heterogeneity parameter	-
V	Volume	m^3
v	Superficial velocity	$m \cdot s^{-1}$
α	Heterogeneity parameter	-
ε	Void fraction	-
ϵ_{rad}	Emissivity	-
η	Effectiveness factor	-
λ	Axial thermal conductivity	$W \cdot m^{-1} \cdot K^{-1}$
ρ	Mass density	$kg \cdot m^{-3}$
τ	Tortuosity	$m_g \cdot m_s^{-1}$
ϕ_{ads}	Thiele modulus for adsorption	-
χ	Max sorbent loading parameter	-

1

Introduction

CO_2 concentrations are rising steadily, posing a significant threat as one of the primary drivers of climate change. The concentration of CO_2 in the atmosphere remained relatively constant at around 280 ppm during the pre-industrial era. During the industrialisation, the concentration increased rapidly to 422.5 ppm in 2024 [49]. In the Paris Agreement in 2015, 196 parties signed a treaty to keep the global average temperature to well below 2°C above pre-industrial levels. Although this goal has been established with so many parties, global emissions still grew slightly more than 0.5% per year, since 2015. Emissions are still increasing, but with a slower rate than before [3]. Bringing this increase to a halt can be done by preventing new emissions or by removing them. In recent years, carbon capture methods that remove CO_2 emissions are gaining more interest.

For some sectors, lowering their carbon footprint is more difficult than for others. Aviation and the steel industry are two of those sectors that have problems in reducing their emissions [10, 39]. Emissions can be roughly divided into point sources, such as those coming from the steel industry, and nonpoint sources, like aviation. Point sources are responsible for around one third of all emissions [30], a potential solution to mitigate emissions for point sources is to use carbon capture and storage (CCS) technologies. With this technology, emissions are absorbed at the outlet stream with increased concentrations of CO_2. CCS is being increasingly implemented, with a total projected capacity exceeding 50 million tonnes per year in 2023 [4]. A different approach should be used for the other two third of emissions.

Sectors like transportation and agriculture, which are highly energy-intensive, emit CO_2 in a dispersed manner. In order to capture these diffuse emissions, various carbon dioxide removal (CDR) methods have been developed, enabling direct CO_2 capture from the atmosphere. The additional advantage of CDR is that it is able to capture the historically emitted CO_2 for scenarios where the temperature increase exceeds 1.5°C. According to the IPCC, the 1.5°C-consistent pathways will be difficult to realize without affordable large scale CDR possibilities, especially in scenarios with an overshoot [27]. Other more natural examples of carbon dioxide removal are storing CO_2 in trees, soils or crops.

In addition to these more natural ways of addressing the problem, there are also a few technical ways, of which direct air capture (DAC) is the most developed [26]. The biggest advantage of DAC compared to the natural methods, is that it requires relative small land areas to capture a tonne of CO_2, and it therefore has a large potential [68]. However, DAC deployment is still on a much smaller scale than other CCS technologies, with 10 kilo tons per year of installed capacity [4]. Significantly more capacity is required to make an impact, especially when compared to the 37,400 million tons of CO_2 emitted in 2023 [3].

Two types of DAC are the most researched: liquid solvent DAC (L-DAC) and solid sorbent DAC (S-DAC). Both have roughly the same energy use, where S-DAC seems to have a lower energy use, but it does require more electricity. Also in costs, the differences are small and a selection of the best performing DAC cannot be clearly made. S-DAC uses temperatures of roughly 100^oC to desorb the CO_2 from the sorbent, while L-DAC needs temperatures around 900^oC to desorb from the solvent. The lower temperatures make S-DAC more convenient for supplying it with renewable energy sources.

Solid sorbent DAC (S-DAC) is described clearly in the paper by McQueen et al. [37]. The biggest company working on this technology is Climeworks, which is used for some reference data. In these systems air is sucked through a contractor unit, where CO_2 and H_2O are adsorbed on the solid sorbent under ambient conditions. This sorbent is a material that bonds well with CO_2, usually amine-functionalised sorbents are used at the surface of the sorbent to enhance selectivity towards CO_2. Once the sorbent is sufficiently saturated with CO_2, the machine is switched to desorption mode where the contactor is closed from the environment. This is generally not continuous, but continuous processes are being researched, with the most potential being a moving bed [43].

There are different modes of desorption. Most commonly used for high working capacities is temperature-vacuum swing adsorption (TVSA). Here the contactor is vacuumed to around 30 mbar, to remove air and then the chamber is heated to release CO_2. This has faster cycle times than just temperature swing adsorption due to the vacuum applied. Steam can also be used to remove CO_2 from the sorbent, which is called steam-assisted TVSA. The steam then passes through a condenser to separate the water, which is captured from the air as a by-product, and CO_2 [69].

To significantly scale DAC, the cost per tonne of CO_2 removed must decrease. It is difficult to determine the price of a novel technology and the cost trajectories for capturing carbon dioxide remain uncertain. Currently the best proven levelized costs of removed CO_2 (LCOD) are the costs from the Climeworks plant, which is \$600/t_{CO_2}, aiming for \$300/t_{CO_2} in 2030 [17]. Cost estimates from \$350/t_{CO_2} [57] and below \$300/t_{CO_2} [38] can be found in literature, as well as estimates below \$200/t_{CO_2} [50]. This is still significantly higher than the current carbon price under the European Trading System (ETS), which is \$65/t_{CO_2} and is expected to rise to \$194/t_{CO_2} by 2035 according to Bloomberg [13]. However DAC costs are expected to decrease as the technology scales up, driven by economies of scale, technological innovation and reduction in operational costs [50].

The largest part of the operational costs from DAC systems, comes from the energy use. The energy use accounts for more than 50% of the levelised cost of CO_2 [22]. Of this energy use, around 80% is used for heating [12]. Reducing energy costs, specifically heating costs, is crucial in reducing total DAC costs. This can be done in two ways; the energy efficiency can be improved by improving processes or by using cheaper forms of energy. Many researchers are already focussing on improving the process with different sorbent materials [51, 56] or different process adjustments [7, 54, 9], trying to maximize the energy efficiency. Others focus more on the energy source used in the process. The costs of combining DAC with small nuclear reactors is proposed [12], as well as waste heat utilisation [38] and photovoltaic (PV) powered DAC [55]. A disadvantage of the latter two is, respectively, the lack of scalability and the need for expensive energy storage.

Another promising approach to reducing operational costs could be to use the heat collected by concentrated solar power (CSP). This is normally used to transform the collected heat into electricity with efficiencies of 40-55% [24], but for the DAC system, it is the heat that is needed. CSP can produce heat for a slightly higher price than PV can produce electricity [8]. The land use is in the same range for electricity production, with some types of CSP performing better than PV [44]. The big advantage of CSP is that it is cheaper to store the relatively high-temperature fluids to account for variations in solar production, than it is to store electricity. The addition of 6-15 hours of thermal energy storage (TES) has already been reported to be considered economical [33].

There are multiple CSP technologies but the main used ones are solar power towers (SPT) and parabolic through collectors (PTC), which have the best performance and the highest temperatures obtained. They do not differ much in costs but SPT uses around 40% more land per installed MW [5]. CSP systems are considered economically viable for electricity production in regions where the direct normal irradiation (DNI) is higher than 2000 kWh·m^{-2}·year^{-1}, but for industrial heat applications, it is already feasible above 1460 kWh·m^{-2}·year^{-1} [18]. Because DAC has high capital costs, it ideally requires a constant stream of heat, which can possibly be delivered better with CSP than with other renewables. Combining the CSP heat with the DAC process can be an interesting way to reduce the costs of DAC, making way for the installation of more DAC plants.

Much research is done on CSP as well as on DAC. However, combining the two is not yet a major research topic. Only a few papers by Prats-Salvado et al. since 2021 have been published about the combination of one specific type of L-DAC and CSP [46, 47, 48]. In this research a constant adsorption process is

proposed with an intermittent energy requiring desorption, to minimise the capital costs. According to Prats-Salvado, the application of CSP and DAC is only proposed, and no techno-economic nor environmental evaluations have been performed before their paper from 2024. Also Wang et al. have conducted some research in combining concentrated solar power to post-combustion carbon capture [66]. The authors find that with using CSP, the costs of removed CO_2 can be similar to the combination with a power plant when thermal energy storage is included. In the paper by Li et al. [34], the authors research if CSP can also be applied to solid sorbent DAC. They state that solar thermal utilization can provide a sustainable heat source for powering DAC, but they do not give many insights in the process since they focus more on the sorbents used.

In order to implement DAC on a larger scale, it is interesting to know all possibilities to decrease the costs of reduced CO_2. Especially the combination of solid sorbent DAC and CSP does not currently have a clear techno-economical assessment. Having this information can drive the acceleration of DAC implementation forwards, leading to a cleaner future.

1.1. Research questions

The primary objective of this research is to evaluate the techno-economic feasibility of a DAC system powered by CSP, in comparison to conventionally powered DAC configurations. This can lead to more impact due to to larger scale implementation. Achieving this could advance efforts toward carbon neutrality or even to a carbon-negative status. To reach this goal, the following research question is defined:

How can CSP and DAC be combined to perform best on the techno-economic aspects: Levelized cost of removed CO_2, land-use and technical feasibility?

In order to answer this main question, the following sub-questions are defined:

- *Which combination(s) of CSP and DAC are most promising, based on the techno-economic parameters?*
- *How can DAC, CSP and TES be combined to perform best on the techno-economic parameters?*
- *How does the combination of DAC, CSP and TES perform on LCOD and land-use compared to other CDR methods?*
- *How does the process perform under variable temperatures, relative humidity and irradiance?*
- *Which properties most strongly influence the LCOD and land-use?*

1.2. Approach

In order to answer the defined research questions, it is necessary to gain some insight in the combination of the processes. This is done by modelling the chosen DAC and CSP types together with TES. In literature, two main methods are used to model DAC. One option is to make a rate-based model with kinetic data, material balance and heat and mass balances, explained in the paper by Driessen et al. [19] and Schellevis et al. [54]. Another option is to have an equilibrium-based model [31]. For S-DAC rate-based models are mainly used because they describes the dynamic behaviour of adsorption better, while for L-DAC the equilibrium-based software Aspen Plus is often used due to its large set of built-in operations, which are convenient for describing the many different processes used in L-DAC. The model approach by Driessen et al. [19] is used as a basis for the development of the model for this research.

The model that is built for DAC is linked to a software that can model the heat input, coming from CSP. The National Renewable Energy Laboratory (NREL) has published an open source software programme to model CSP. The System Advisor Model (SAM) is used for techno-economical analysis and is used for dimensioning the CSP part. It also comes with heat storage calculation possibilities, which is used as well.

Once the models are combined by using the collected heat as input for the DAC desorption, the DAC model gives the hourly adsorption and desorption rate, which depends on CO_2 concentrations, relative humidity and temperature. This is linked to the CSP heat production to get to the amount of captured CO_2. With this amount of CO_2 removed and the costs of the whole plant, the LCOD is determined. By changing the thermal storage size and the size of the solar field, the optimum configuration with the lowest LCOD is determined.

The found optimal configurations are broken down in their cost components and the sensitivity of the major determining components is determined. This gives a more realistic insight into the uncertain costs. The amount of aperture area of the solar collectors required per tonne CO When the LCOD and land-use are known, this can be compared to other technologies found in literature. The input parameters are changed to see what influence temperature, humidity CO_2 concentrations and irradiance will have on the LCOD and land-use.

2

Methods

2.1. Physics of Adsorption

A rate-based model is best for the case of adsorption because of the rate-based adsorption process. Often adsorption is simplified to changes in just one of the two directions in which effects occur. This is done in the radial dimension of the particles such as in [19], or on the reactor length scale of the reactor [58]. An effort was made to develop a more computationally efficient 0D model, which is elaborated in Appendix A. Ultimately, the computational time was found not be prohibitive, so the 1D approach in the reactor length scale was used for the remainder of the work.

The DAC model approach by Driessen et al. [19] is used as the basis for the development of the model for this research. The authors used an often used amine sorbent in literature called Lewatit VP OC 1065 (hereafter referred to as Lewatit), and to easily validate the data, this sorbent is used as well. Lewatit is a polymeric resin functionalised with primary amines, and is believed to be very similar to the adsorbent used by Climeworks and is often used as a benchmark adsorbent [35]. CO_2 adsorbs to this surface due to chemisorption, which forms a strong bond, while H_2O on the other hand, adsorbs due to physisorption. This amine sorbent is advantageous because the H_2O does not have competitive desorption with CO_2, but it enhances the CO_2 capacity [64]. Most studies suggest that a moderate amount of H_2O is beneficial to the process, but the exact influence that the RH has is still being researched [52].

The described approach is the Thiele modulus approach with the approximation of a uniform loading profile. This model takes into account these particle-level processes without having to discretize the reactor in 2 dimensions. This model requires numerical integration only in the length direction, by adding the radial resistance as an effectiveness factor that decreases the sorbent loading rate.

2.1.1. Sorbent Loading CO_2

Chemisorption of CO_2 is modelled with the Toth isotherm [20], [19]. With the Toth isotherm, the equilibrium sorbent loading (q^*) at a specific pressure and temperature is calculated:

$$q^* = \frac{q_s b p_{CO_2}}{(1 + (b p_{CO_2})^{t_h})^{\frac{1}{t_h}}} \tag{2.1}$$

Here q_s is the maximum sorbent loading at any pressure, t_h is the heterogeneity parameter and p the pressure. The parameters b, t_h and q_s are temperature dependent:

$$b = b_0 \exp\left(\frac{-\Delta H}{R T_0}\left(\frac{T_0}{T} - 1\right)\right) \tag{2.2}$$

$$t_h = t_{h_0} + \alpha\left(1 - \frac{T_0}{T}\right) \tag{2.3}$$

$$q_s = q_{s_0}\, exp\left(\chi\left(1 - \frac{T}{T_0}\right)\right) \tag{2.4}$$

Here ΔH is the isosteric heat of adsorption at zero fractional loading, α and χ are dimensionless parameters and R is the gas constant. The Toth isotherm is converted to a reaction rate R_a [19]:

$$R_A = \frac{\delta q}{\delta t} = k_T \left(\left(1 - \left(\frac{q}{q_s}\right)^{t_h}\right)^{\frac{1}{t_h}} RTc - \frac{q}{bq_s}\right) \tag{2.5}$$

Here k_T is the reaction rate constant. This rate is dependant on the activation energy (E_{act}), the rate at $T = 0$ (k_0) as well as the temperature. This reaction rate is obtained with the Arrhenius equation:

$$k_T = k_0 \cdot \exp\left(\frac{-E_{act}}{RT}\right) \tag{2.6}$$

An isotherm that takes into account the RH of the gas is the weighted average dual-site Toth (WADST) isotherm, which performs best according to experimental tests from Chimani et al. [15]. This is an isotherm based on the Toth isotherm that takes into account the availability of the water molecules at sites on the adsorbent. In the end, this method was not used because of the lack of available parameters for the reaction rate.

2.1.2. Sorbent Loading H_2O

The multilayer physisorption of H_2O on the amine is described with the Guggenheim Anderson de Boer (GAB) model [64]. The GAB isotherm is given as:

$$q^* = \frac{q_{mono} C K (p/p_s)}{(1 - K(p/p_s))(1 + K(p/p_s)(C - 1)} \tag{2.7}$$

Here q_{mono} is the monolayer adsorption capacity of H_2O and C and K are temperature-dependent parameters:

$$C = C_0 \, \exp\left(\frac{\Delta H_c}{RT}\right) \tag{2.8}$$

$$K = K_0 \, \exp\left(\frac{\Delta H_k}{RT}\right) \tag{2.9}$$

Where ΔH_c and ΔH_k are respectively adsorption enthalpies of monolayer and multilayer adsorption. It has been proven many times, that the adsorption of H_2O is much faster than for CO_2 [16], [67], [54]. Therefore, the reaction kinetics of the sorbent loading of water do not have to be calculated for adsorption, since it is fully saturated at the end of the adsorption cycle. For desorption, the H_2O desorption rate is necessary because it influences the temperature. The kinetics are described by a first-order linear driving force. The values used to describe this are obtained from Schellevis et al. [53] displayed in Table 2.1.

2.1.3. Diffusion Limitations

A modified version of the Thiele modulus (ϕ_{ads}), assuming a uniform sorbent loading profile, is used to relate intra-particle diffusion limitations to exterior surface conditions, proposed by Driessen et al. [19]. This effectiveness factor is equal to 1 for desorption, as the sorbent is loaded above its equilibrium under these conditions, and when the sorbent is at equilibrium the effectiveness factor limit of 1 is reached. The modified Thiele modulus is given as:

$$\phi_{ads} = \phi^* \sqrt{(1 - q'^{t_h})^{1/t_h}} = r_s \sqrt{\frac{\rho k_T RT (1 - q'^{t_h})^{1/t_h}}{D_p}} \tag{2.10}$$

Table 2.1: Model parameters for CO_2 desorption on Lewatit VP OC 1065 from Schellevis et al. [54] if not otherwise indicated

Section	Parameter	Value	Unit
Toth isotherm	q_{s0}	3.40	$mol_{CO_2} \cdot kg^{-1}$
	χ	0	-
	T_0	353.15	K
	b_0	$93.0 \cdot 10^{-5}$	Pa^{-1}
	ΔH_0	95.3	$kJ \cdot mol_{CO_2}^{-1}$
	t_0	0.37	-
	α	0.33	-
Toth kinetics	k_{0,CO_2}	$3.5 \cdot 10^3$	$mol_{CO_2} \cdot kg^{-1} \cdot bar^{-1} \cdot s^{-1}$
	E_{act,CO_2}	15.2	$kJ \cdot mol^{-1}$
GAB isotherm	q_{mono}	5.55	$mol_{H_2O} \cdot kg^{-1}$
	$C_{0,GAB}$	100	-
	$k_{0,GAB}$	0.92	-
	ΔH_c	-8.69	$kJ \cdot mol_{H_2O}^{-1}$
	ΔH_k	-0.82	$kJ \cdot mol_{H_2O}^{-1}$
GAB kinetics	k_{0,H_2O}	450	s^{-1}
	E_{act,H_2O}	15.2	$kJ \cdot mol_{H_2O}^{-1}$
Transport and structure	D_{AB}	$1.67 \cdot 10^{-5}$	$m^2 \cdot s^{-1}$
	ε_s	0.23	$m^3 \cdot m^{-3}$
	ε [42]	0.375	$m^3 \cdot m^{-3}$
	τ	2.3	$m \cdot m^{-1}$
	ρ_s	880	$kg \cdot m^{-3}$
	r_s	$334 \cdot 10^{-6}$	m
	d_p	668	µm

Here q' is the nondimensionalized sorbent loading and r_s is the particle radius. The term D_p is the effective pore diffusion coefficient, which is calculated as:

$$\frac{1}{D_p} = \frac{\tau}{\varepsilon_s}\left(\frac{1}{D_{AB}} + \frac{1}{D_{Kn}}\right) \tag{2.11}$$

In this equation ε_s is the particle porosity and τ is the tortuosity of the medium. The molecular diffusion coefficient D_{AB} is proportional to $T^{1.75}$. The Knudsen diffusion coefficient D_{Kn} is defined as:

$$D_{Kn} = \frac{d_{pore}}{3}\sqrt{\frac{8RT}{\pi M_{CO_2}}} \tag{2.12}$$

Where M_{CO_2} is the molar mass of CO_2. With the definition of the Thiele modulus for adsorption, the effectiveness factor is calculated:

$$\eta_{ads} = \frac{3}{\phi_{ads}}\frac{(\phi_{ads} coth(\phi_{ads}) - 1)}{\phi_{ads}} \tag{2.13}$$

The effective reaction rate is:

$$R_{A,ef} = \eta_{ads} R_A \tag{2.14}$$

2.1.4. Mass Balances

The mass balance for the gas phase of adsorption and desorption is described by:

$$\varepsilon\frac{\partial c}{\partial t} = -\frac{\partial (vc)}{\partial x} - (1-\varepsilon)\rho_s \sum_{i=1}^{n}\frac{\partial q}{\partial t} \tag{2.15}$$

Here ε_s is the void fraction of the bed. For adsorption the term $\frac{\partial (vc)}{\partial x}$ reduces to $v\frac{\partial (c)}{\partial x}$ because the velocity is assumed to be constant because of the small concentrations of CO_2 and H_2O removed from the flow.

In order to solve this and other partial differential equations, the method of lines is used. This method discretises the spatial dimension into smaller sections in a staggered grid. This makes it possible to reduce it to a system of ordinary differential equation, which is numerically easier to solve. All ordinary differential equations are solved with the LSODA method, which solves stiff and non-stiff problems. The convective term is discretised with a first-order upwind scheme.

During adsorption, the change of the total mass of the gas phase is negligible, allowing to treat the gas velocity as constant. During desorption at decreased pressure, this is no longer valid. The desorption of CO_2 and H_2O influences the flow so that it either increases the velocity or the pressure of the gas. The method from Schellevis et al. [54] is used where the gas velocity is taken to change, since the pressure drop is negligible compared to the total pressure. The mass balance becomes:

$$\varepsilon \frac{\partial c}{\partial t} = -\frac{\partial (vc)}{\partial x} - (1-\varepsilon)\rho_s \sum_{i=1}^{n} \frac{\partial q}{\partial t} \tag{2.16}$$

The total velocity increase for desorption is significant. This is the sum of the CO_2 and H_2O contribution. Only for this calculation the concentration differences of both gases is taken together. This increase is calculated by calculating the maximum concentration with the ideal gas law and inserting this into the equation above. It is then be rewritten to the form:

$$-\frac{\varepsilon p}{RT^2}\frac{\partial T}{\partial t} = -\frac{p}{R}\frac{\partial (\frac{v_g}{T})}{\partial x} + (1-\varepsilon)\rho_s \left(\frac{\partial q_{H_2O}}{\partial t} - \frac{\partial q_{H_2O}}{\partial t} \right) \tag{2.17}$$

Which is rewritten to:

$$\frac{\partial (\frac{v_g}{T})}{\partial x} = \frac{\varepsilon}{T^2}\frac{\partial T}{\partial t} - (1-\varepsilon)\frac{\rho_s R}{p} \left(\frac{\partial q_{H_2O}}{\partial t} + \frac{\partial q_{H_2O}}{\partial t} \right) \tag{2.18}$$

A first-order upwind scheme is used to discretize the velocity terms. Integrating Equation 2.18 over the length with the cumulative trapezoidal rule and multiplying it by T gives the velocity increase that is added to v_{purge}.

2.1.5. Energy Balance

The thermal energy balance is only considered during desorption, and is based on the method by Schellevis et al. [54]. The heating is assumed to be uniform. Temperature gradients are taken into account for heat transfer in the axial direction. The heating is assumed to be constant everywhere at the surface of the bed.

$$\begin{aligned} ((1-\varepsilon)\rho_s C_{p,s} + \varepsilon \rho_g C_{p,g}) \frac{\partial T}{\partial t} &= \frac{\partial}{\partial x}\left(\lambda \frac{\partial T}{\partial x} - v\rho_g C_{p,g} T \right) \\ &+ (1-\varepsilon)\rho_s \left(\Delta_r H_{CO_2} \frac{\partial q_{CO_2}}{\partial t} + \Delta_r H_{H_2O} \frac{\partial q_{H_2O}}{\partial t} \right) + a_s h_t (T_{ht} - T) \end{aligned} \tag{2.19}$$

The derivative $\frac{\partial^2 T}{\partial x^2}$ is calculated with a central difference scheme, because it represents conduction. However, the other derivative $\frac{\partial T}{\partial x}$ represents a convection term, calculated with a first order upwind scheme because it is driven by advection. The assumption is made that the temperature of the gas is similar to the temperature of the sorbent at the corresponding cell. The thermal properties of Lewatit are shown in Table 2.2.

Boundary Conditions

A zero-gradient Neumann condition is applied at both the inlet and outlet boundaries for adsorption. The initial sorbent loading is dependent on the result of the desorption model. The initial concentration is set

Table 2.2: Physical properties of Lewatit VP OC 1065

Parameter	Value	Unit
$C_{p,s}$	1580	J·kg^{-1}·K^{-1}
λ_{ax}	0.121	W·m^{-1}·K^{-1}
$\Delta_r H_{CO_2}$	1.7	MJ·kg^{-1}
$\Delta_r H_{H_2O}$	2.4	MJ·kg^{-1}

equal to the outgoing concentration (c_{out}) everywhere. Only at the point $x = 0$, the concentration has to be c_{in} at all times.

The desorption model is less numerically stable than the adsorption model and therefore requires carefully selected boundary conditions to minimise instabilities. For this purpose, Danckwerts boundary conditions are applied [54], as they are suited for systems involving both advection and diffusion. These boundary conditions are defined as follows:

$$-D_{ax}\left.\frac{\partial c}{\partial z}\right|_{z=0} + uc|_{z=0} = u_{in}c_{in} \tag{2.20}$$

$$-\lambda_{ax}\left.\frac{\partial T}{\partial z}\right|_{z=0} + u_g\rho_g C_{p,g}T|_{z=0} = u_{in}\rho_g C_{p,g}T_{in} \tag{2.21}$$

In the case of concentration, the boundary condition has to be applied for both H_2O and CO_2. For the outlet the gradients are all equal to zero. The starting values of the concentrations, sorbent loading, and temperature depend on the final conditions of the previous adsorption cycles.

2.1.6. System Settings

In order to create a 1000-tonne-per-day DAC system, the DAC unit is oversized to take the less than 100% capacity into account. The DAC system modelled here is based on the one-kilogramme-per-day system described by Schellevis et al. [54]. The bed thickness is kept similar to avoid a large pressure drop. The total cross sectional bed area is increased to scale the system to the required size. The used dimensions are summarized in Table 2.3. The cycle times used are not including the time it takes to evacuate and cool the bed since no calculations are being done for these steps. It is assumed this takes 10 minutes total, leading to cycle times of 200 minutes.

In this research, the hourly changes in humidity and temperature of the Almeria location, Spain, are used from the typical meteorological year. Later this is also compared to Alice Springs in Australie, a location with better performance. The CO_2 concentration is taken to be constant at the most recent reported yearly average of 422.5 ppm [3]. These hourly climate conditions are calculated for all possible combinations in Almeria and Alice-Springs rounded to 5K and 0.1 relative humidity. Since there are many DAC units which are not all in the same phase, it is assumed that the conditions calculated for the hourly climate conditions are the real energy use for that hour. This is not exactly true since the cycles take 200 minutes, but the relative small temperature and humidity changes over 200 minutes makes it valid. The assumption decreases the computational time significantly because it reduces the possible cycles notably.

From the output of the total cycle, a formula is fitted to calculate the sorbent loading of CO_2 at the end of the desorption cycle as a function of RH. This is not done for water because the kinetics do not determine the final sorbent loading here. This fit is used to get the initial conditions for the adsorption. This is not perfect, because the initial conditions are now determined by its own output, but it gives the best start condition without having to calculate every cycle with different initial conditions. This quadratic fit is has a R-squared of 0.988:

$$q_{0,CO_2} = 0.7464 \cdot RH^2 - 0.4812 \cdot RH + 0.24 \tag{2.22}$$

Table 2.3: System dimensions of DAC, based on Schellevis et al. [54] with increased cross sectional area by using multiple DAC units

Parameter	Value	Unit
Bed thickness	2.4	cm
Cross sectional area	$3.3{\cdot}10^5$	m^2
Sorbent mass	5000	tonnes
Adsorption time	150	min
Desorption time	30	min
Heating time	10	min
Desorption pressure	7400	Pa
Superficial gas velocity ads	0.15	$m{\cdot}s^{-1}$
Purge rate	0.87	$g_{st}{\cdot}min^{-1}{\cdot}kg_s^{-1}$
Void fraction particles	0.4 [42]	-
CO_2 concentration	422.5 [3]	ppm

2.1.7. Model Validation

Due to the difficulty in measuring the loading of the sorbent over time, verification is carried out with CO_2 breakthrough curves: the gas phase concentration over time measured at the outlet during an adsorption experiment. In Figure 2.1 are two breakthrough curves with which the model is verified. The data is also validated with a sorbent loading measurement in Figure 2.2, which also corresponded very well. The variable dimensions of the different reference data are summarised in Table 2.4.

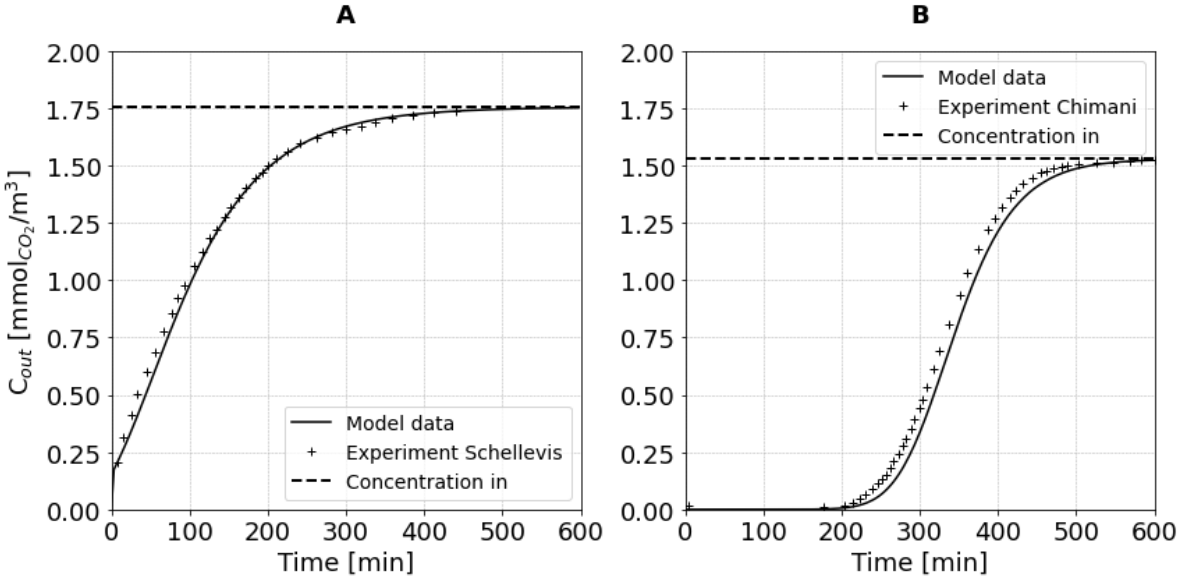

Figure 2.1: Breakthrough curve validation of the model created with data from A: Schellevis et al. [54] and B: Chimani et al. [15]. Parameters used in the measurements are summarised in Table 2.4

Desorption Temperature Profile

Contrary to adsorption, no applicable loading data is available during desorption. Therefore, instead the bed temperature is compared to data reported by Schellevis et al. in Figure 2.3. It is clear that at the end the temperature is overestimated but before that, it has a good match. This is probably caused by losses to the environment that are not added in the model as well as higher conductive losses in reality because of the sorbent with poor heat conduction characteristics. The conditions used are stated in Table 2.3.

The results show a working capacity of 1.1 mol_{CO_2} kg_s^{-1} for CO_2 and 0.5 mol_{H_2O} kg_s^{-1}, while it is respectively 0.92 and 1.02 in the article. However, the water loading at the start of desorption is 1.82 mol/kg, while the final equilibrium loading at desorption conditions is 1.22 mol_{H_2O} kg^{-1}, meaning the working capacity is limited to 0.6 mol_{H_2O} kg^{-1}. It is impossible to have a higher working capacity at these conditions, which means that the initial conditions might have a higher relative humidity than the unclear stated values in the article. The energy requirement is compared with an energy assessment from Sabatino et

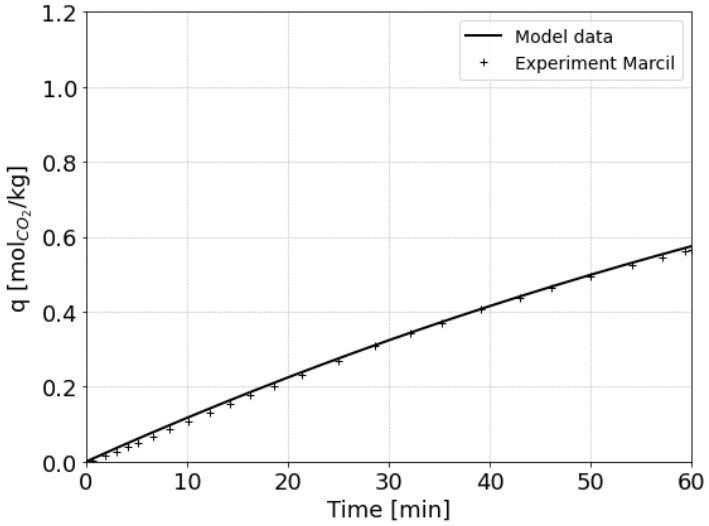

Figure 2.2: Sorbent loading validation with data from Marcil et al. Parameters used in the measurements are summarised in Table 2.4 [36]

Table 2.4: Parameters used in the validation models, every model is at atmospheric pressure

Parameter	Schellevis	Chimani	Marcil
L [m]	0.024	0.05	1.5
A [m^2]	0.126	0.0178	0.035
T_{ads} [^{o}K]	293	303	289
c_{in} [ppm]	420	380	420
Q_{gas} [m^3·h^{-1}]	67.9	6	1500
q_o [mol·kg^{-1}]	0.2	0	0
RH [-]	0.5	0.35	0.45

al. [50]. For the same sorbent Lewatit and design conditions of 0.43 relative humidity and 400 ppm$_{CO_2}$, this led to a specific energy use of 1.3 MJ kg$^{-1}_{CO_2}$ for CO_2 and between 4.2-6.3 MJ kg$^{-1}_{CO_2}$ for H_2O, for respectively minimum exergy consumption and maximum productivity.

Adsorption Cycle Time

It can be seen in Figure 2.4 that the equilibrium sorbent loading decreases with temperature, but the sorbent loading at the end of the adsorption cycle is relatively constant up until 295 K where it starts to decrease. In Figure 2.5 the temperature distribution is given for Almeria, the temperatures lay between 285-305^{o}K and are most frequently at 290 K. At 290 K the sorbent is loaded for more than 75%. The cycle times are a trade off, where high sorbent loading is beneficial, but the expensive capital costs require high rates. When looking back at the sorbent loading over time for the correct reactor dimensions in Figure A.6, it can be seen that at a sorbent loading of 75%, the intrinsic adsorption rate is starting to decrease significantly. The cycle time is not optimised in this research, but this indicates that the fast adsorption from the start is at least passed and it would be a waste to stop adsorption before that started to decrease. The other temperature that occurs often is 300 K. At this temperature the sorbent is loaded for 93%. Checking this value with the same sorbent loading curve, the rate is not yet in the stage where it becomes close to 0, so it is still adsorbing at the end, and the adsorption time does not have to be decreased.

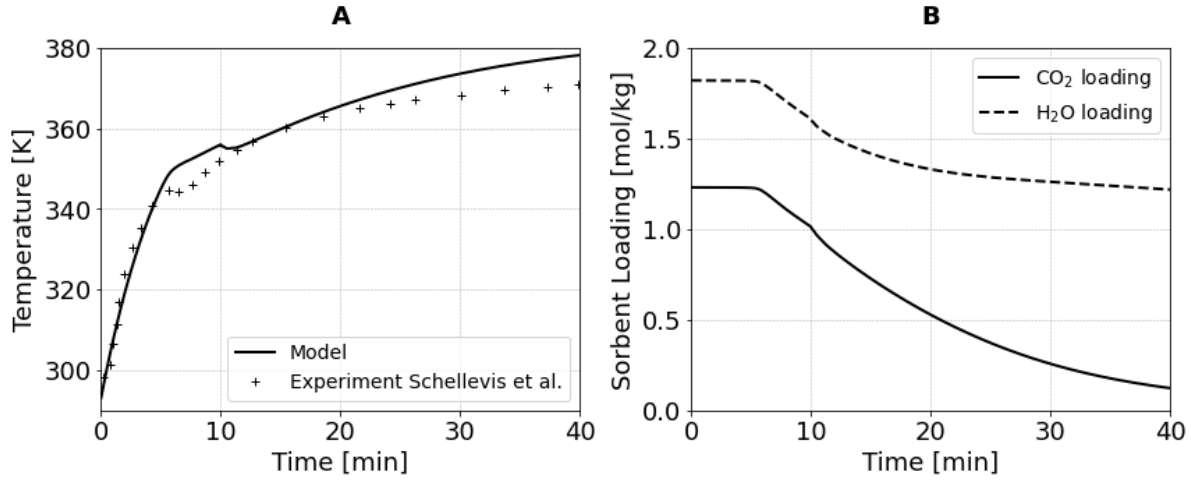

Figure 2.3: Desorption validation with data from Schellevis et al. [54] in fig A and the belonging sorbent loadings in B . At 10 minutes the purge is started. The hot fluid temperature is 383K and the adsorption relative humidity is 0.19

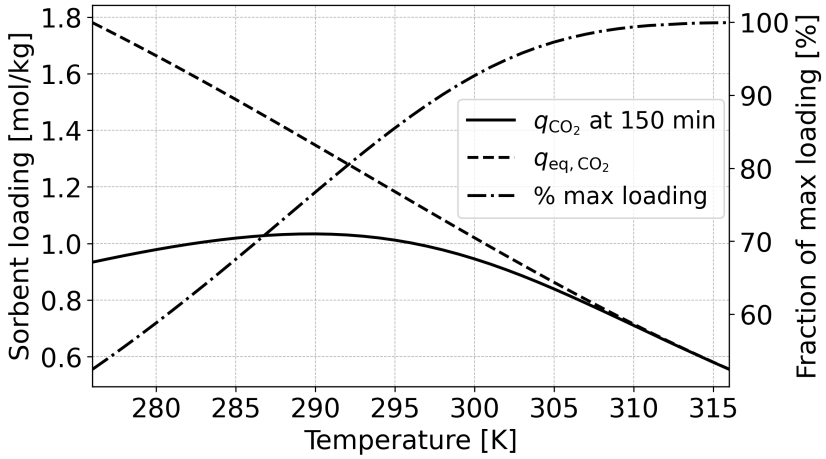

Figure 2.4: Influence of temperature on adsorption sorbent loading and kinetics. The equilibrium sorbent loading is plotted as well as the sorbent loading after an adsorption cycle of 150 min. The fraction of the maximum sorbent loading is plottes as well. It can be observed that the equilibrium value decreases with temperature while the kinetics increase

2.2. Modelling Concentrated Solar Power

Two types of CSP are investigated, namely Parabolic Through Collectors (PTC) and Solar Power Towers (SPT). For SPT the radiation is received in a big field of mirrors called heliostats, which all point to a large central receiver tower. PTC systems have U-shaped mirrors with large receiver tubes between them, on which the radiation is focussed. Both systems have tracking systems to optimally direct the radiation to the receiver. The receiver tubes are insulated with a vacuum tube at the outside to limit the heat losses, which can be significant due to the large contact area with air. Both systems require active control in order to optimise the mirror angles and with that the heat produced, PTC only tilts in one axis while SPT tilts in two directions. Defocussing is also used to lower the heat of the system when it is exceeding the limits [28].

For this study a DAC system of 1000 tonnes per day is chosen. This DAC plant size requires a CSP power of roughly 100 MWp. The techno-economic performance of CSP is evaluated using the System Advisor Model (SAM) [41]. The goal is to design a CSP system with the lowest LCOD when combined with the DAC system. Therefore two parameters are optimised: the solar multiple (SM), which is the ratio of the heat collected at maximum incoming radiation to the heat demand of the DAC block; and the hours of thermal storage (HS), which is the amount of hours the DAC demand can be delivered by the thermal storage.

The base case scenario is that the DAC and CSP together are a stand-alone system, without energy surplus or deficiency. This makes it a realistic scenario that can be implemented in many locations, while losing the potential economical benefit of the high temperature waste heat. Two locations with different properties are researched. One being Almeira in Spain, since Spain is one of leading countries in the development of CSP and it has a suitable climate for this. The second location is only being used to see the effect of a more continuous radiance profile on the performance. Alice Springs in Australia is chosen as the location with more radiation and a more constant profile.

2.2.1. Physics of Concentrated Solar Power

Both PTC and SPT systems are modelled very similar. For calculating the incoming heat, direct normal irradiance (DNI) is used as input parameter. This is the amount of irradiation over a surface perpendicular to the rays, that is optimally the direction in which collectors are placed. For the heat losses the ambient temperature is important as well, the probability density functions of these parameters, as well as the humidity which is more important for DAC, are shown for Almeria in Figure 2.5 and Alice Springs in Figure 2.5. These values come from the typical meteorological year, which is a combination of months from different years that represent the best average for that location. When this DNI is multiplied with the aperture area (A_{ap}) of the collector, which is the area of the collectors perpendicular to the radiation, the amount of energy that the rays exert on the surface is obtained.

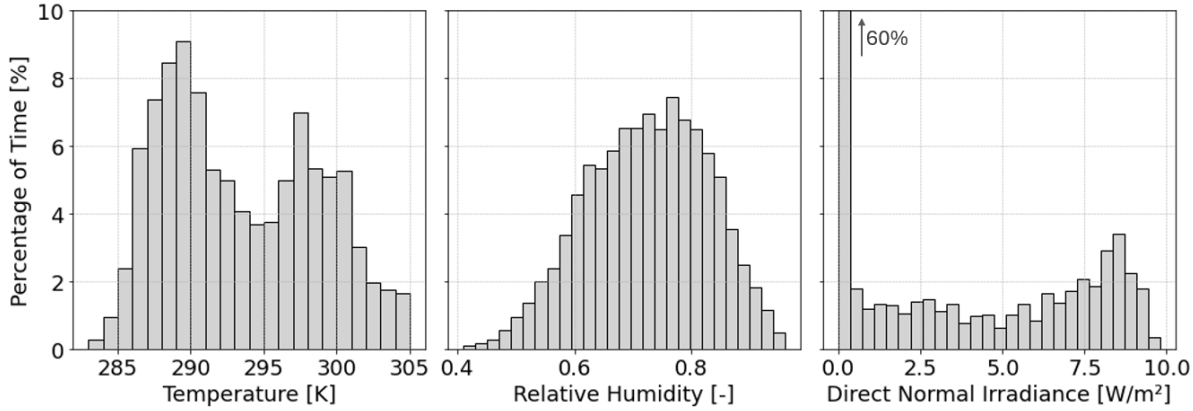

Figure 2.5: Probability density function of the temperature and RH of Almeria for the typical meteorological year. The first DNI bin is 60% but is cut off at the top for better readability

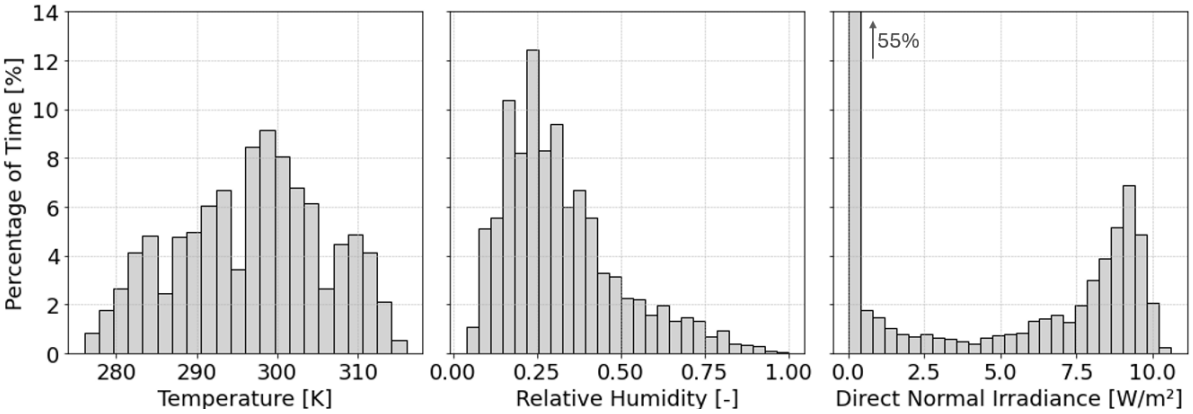

Figure 2.6: Probability density function of the temperature and RH of Alice Springs for the typical meteorological year. The first DNI bin is 55% but is cut off at the top for better readability

Ideally the collectors reflect all the energy to the receiver, but in reality the mirrors do not reflect all the energy. Part of the incoming energy is transformed to heat in the mirror, some parts of the mirror also have dirt, which reflects less of the radiation. Part of the radiation is also lost due to misalignment due to imperfect mirror shapes and a part is lost due to errors in tracking. All of these efficiencies are summarised in the collector efficiency η_c.

Receivers also have some efficiency losses. These are due to the receiver not being a perfect absorber, as well as the temperature increase which leads to the emittance of radiation as well. The coating of the receiver therefore ideally has a very high absorptance (α) while having a low emissivity (ϵ_{rad}). Lastly the tube suffers from some convective heat losses, even with the glass tube around it at a vacuum.

A large loss factor is determined by the cosine losses of the system. This is caused when the sun has a small horizontal angle, which leads to collectors shadowing other collectors. The system is assumed not to work when these losses are larger than 50%, occurring around dusk or dawn.

The outgoing radiation is not discussed in its full complexity, but it can be reduced to a receiver efficiency η_r. This is reduced to a 1D radial thermal resistance network, where different convective and radiative terms are added. When starting up and shutting down, the temperatures of the components such as the receiver and vacuum tube change depending on their specific heat capacities and incoming energy. For an in-depth explanation of the calculations executed by SAM, the reader is referred to the SAM technical manual [65].

All the losses combined give the heat balance for the receiver, where Q_{abs}, the absorbed heat by the heat transfer fluid(HTF), and the heat loss from the receiver (Q_{out}) are not specified:

$$DNI \cdot A_{ap} \cdot \eta_c \cdot \eta_r \cdot \epsilon_{rad} = Q_{out} + Q_{abs} \tag{2.23}$$

For the thermal energy storage, a two tank system is used with a heat exchanger in the PTC and without one for SPT, sized with the $\varepsilon - NTU$ method, to transfer heat from the field to the tanks. The size required for these tanks is calculated based on the defined hours of thermal storage. The heat losses are dependant on time and for every time step the temperature of the storage fluid is calculated.

2.2.2. System Control

SAM makes sure that the loop outlet temperature is at the required temperature when possible, by changing the mass flow rate. The minimum and maximum flow rate are defined in the user interface. In the case where too much heat is produced for the system to handle, the collectors are simultaneously partially defocussed to avoid dangerous temperatures.

When there are longer periods of shutdown during nights for example, the HTF can drop in temperature to unacceptable temperatures where freezing can occur. The TES tank is also heated to prevent freeing when necessary. The heat that is required to avoid this, is given as a parasitic loss. The second large parasitic loss is the electricity required for the pumping of the fluids through the system. The pressure drops are calculated on the basis of the diameters and pressure drop factors for components such as elbows, valves, etc., as well as expansions and contractions, which are minimised for the required flow boundaries. Diameters are chosen such that the minimum and maximum chosen flow velocities are maintained at design conditions.

2.2.3. SAM Simulations

SAM has been validated against international benchmarks and real-world performance data. It shows good agreement with the SolarPACES guidelines [32], developed by a network of research institutions under the IEA. Case studies of the Andasol-1 PTC plant and the Gemasolar SPT plant demonstrate that SAM predicts annual energy output within approximately 3% of measured values [1, 2]. Additionally, third-party validation by Boretti et al. [14] for four plants states that PTC is very close with the measured values, though it highlights discrepancies for SPT. While SAM is not without limitations, particularly for solar towers, it provides proper insight for techno-economic analysis and preliminary system design.

The CSP methods in SAM are initially created to get an electricity output from a power cycle, the system is schematically given in Figure 2.7. The Industrial Process Heat performance model is based on this model, but without the power cycle. One very important input on which the model is based is the solar input file per time step, which is in this case one hour. From the cumulative density function of the irradiance, the design point direct normal irradiation (DNI) is determined, which falls below 900 W·m^{-2} 95% of the time for Almeria.

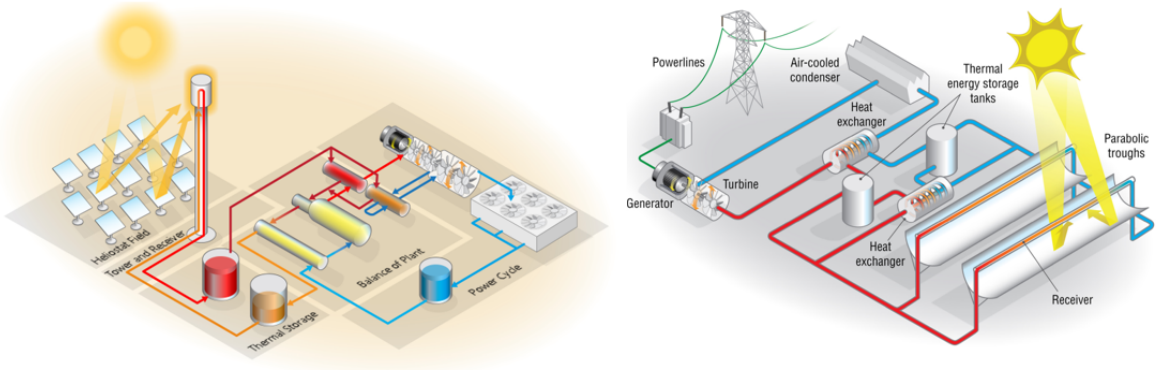

Figure 2.7: Default SAM system for SPT (left) and PTC (right). The SPT has a heliostat field that directs radiation to the tower with receiver. Both systems have two thermal storage tanks for hot and cold fluids, but in the PTC a heat exchanger is used because of the different fluids in the receivers and in the thermal storage. The image contains a power cycle but that is not the case for the used industrial process heat system. The image is licensed under the BSD 3-Clause License and developed by the National Renewable Energy Laboratory (NREL)

Heat Transfer Fluid

The heat transfer fluid (HTF) selection determines the temperature range and the specific heat of the fluid and thereby required flow rates and tubing sizes. In general the most prevalent choice is for SPT to use molten salts and for PTC to use thermal oils, where Therminol VP-1 is an industry standard [28]. This is because SPT concentrates the radiation more, making it possible to produce higher temperatures, and more economical TES. PTC has large tubing that needs to be protected from freezing, using a fluid that solidifies at ambient temperatures, such as molten salt is therefore inconvenient. Temperature limits are defined that limit the HTF in order to avoid freezing or corrosive behaviour. Therminol is limited between 20-400°C and the solar salt between 280-500°C.

Total Power

Controlling the system for both electricity and heat at the same time is impossible in SAM. This is solved by over-sizing the heat requirement of the DAC system, to account for the electricity need of both the solar plant and the DAC system. With the assumptions listed in Table 2.6. This is calculated by calculating the fraction of the total power that is needed for heat (H) based on a constant power cycle efficiency. One minor addition has to be made to obtain the final energy use, and that is that the CSP plant uses electricity itself, which also changes per configuration. The results show the electrical energy use of the CSP plant to be approximately 2% of the thermal production for the studied cases. The total system power is then calculated with the factor H, the required rated power for the 1000 tonnes per day DAC system is 372 MWt.

$$1 = (H + \frac{E_{el}/E_{th} \cdot H}{\eta_{PC}}) \cdot (1 + \frac{0.02}{\eta_{PC}}) \tag{2.24}$$

$$P_{total,system} = \frac{E_{thermal} \cdot m_{CO_2}}{24 \cdot H} \tag{2.25}$$

The weather conditions determine the power that the DAC system requires per hour, this is modelled as a capacity factor of heat that the CSP system delivers to the DAC system. This is added to SAM as a list of factors, limiting the maximum supplied output. Because of this hourly varying limit, the capacity coming out of SAM is not equal to the DAC capacity. The capacity from SAM is divided by the average maximum capacity of the DAC system, to get the capture capacity. With that limitation, the capacity and LCOH are used to obtain the lowest LCOD configuration values for the CSP and TES system. The real amount of tonnes of CO_2 produced is calculated at the optimal point with hourly energy requirement.

Collector and Receiver

Both the receivers and collectors are selected from industrial standards. For the receiver a Schott PTR80 is chosen with a SkyFuel SkyThrough with 80 mm OD receiver. For Therminol the default values for heat

loss in the receivers is taken. All the collectors are put in loops from the main piping, the amount of collectors in a loop are defined and set to 20, because this resulted in the lowest parasitic losses.

For the SPT system, the heliostat field and receiver height is optimised for the lowest levelised cost of electricity with the SolarPILOT^{TM} software. This calculates the optimal receiver dimensions and height from the ground, as well as the number of heliostats and their placement based on their defined dimensions and placement limitations. Optimisation is performed for all situations.

Thermal Energy Storage

Since the CAPEX of the DAC system are so high, it is desired to have a constant supply of heat to make optimal use of the DAC equipment. This requires high solar multiples to be able to fill the TES. Overall the high solar multiples of more than 7 seemed to lead to unrealistic behaviour, where the capacity decreased for the same hours of storage and an increasing solar multiple. For PTC the cold tank temperature set point is set to 100°C to avoid dispatching temperatures that are too low to heat the sorbent, this is not necessary for SPT which is already limited by the high freezing temperature of molten salt.

2.3. Energy Requirement DAC

The sorbent loading and temperatures serve as the input for the energy calculations. Based on the hourly sorbent loading profiles, the influence of temperature on adsorption and relative humidity on desorption is mapped. Note that the influence of RH on CO_2 adsorption is not taken into account in this model, but the RH at the adsorption stage does determine the amount of water that gets desorbed, which leads to an energy penalty during desorption. This data is based on the paper by Schellevis et al. [53]. Because energy demand is highly dependent on climate, it is important to know the temperatures and RH of the examined location, which are shown in Figure 2.5.

2.3.1. Electrical Demand

Both adsorption and desorption are modelled with a constant cycle time. This makes it easier to model. In reality this can be optimised when temperature and relative humidity are measured and used to model optimal performance, this is beyond the scope of this research. During adsorption, the fan power is constant and the cycle time is also constant. The fan energy and the vacuum pump together determine the electrical requirement. These values are independent of weather conditions and therefore constant.

The setup from the reference paper gives a compression energy requirement and a vacuum requirement. They are respectively 0.34 and 0.46 MJ $kg^{-1}_{CO_2}$, but that is dependent on the CO_2 sorbent loading. With a reported working capacity of 0.92 mol_{CO_2} kg_s^{-1} per cycle at the tested ambient temperature, this is 0.041 kg_{CO_2} kg_s^{-1}, so 14 and 30 kJ kg_s^{-1} for respectively compression and evacuation. It is defined per kg sorbent because it scales linearly with the mass when the same thickness of the bed is kept. This is in line with the article from Sabatino et al. [50] where a slightly lower vacuum of 0.1 bar is used.

2.3.2. Thermal Energy Demand

The amount of CO_2 and H_2O multiplied by their reaction heats, gives the heat that is needed to break the bonds of the sorbent with CO_2 and similarly for H_2O:

$$E_{ads,CO_2} = \Delta_r H_{CO_2} \cdot \Delta q_{CO_2} \cdot m_s \tag{2.26}$$

The heat that is lost as sensible heat to the reactor is dependent on many factors, such as the material and insulation. For their setup, Schellevis et al. report a heat loss of 186 kJ kg_s^{-1}, but this is lowered by heat integration and better insulation to 41 kJ kg_s^{-1}. The energy requirements independent of weather are given per kg of sorbent per cycle, converted with the working capacity per cycle, which is 0.92 mol_{CO_2} $cycle^{-1}$ times the mole mass of CO_2. The thermal energy used to heat the sorbent is dependent on the mass and the temperature difference during heating. Lewatit has a specific heat of 1580 J kg^{-1} K^{-1}. This is expressed as:

$$E_{sorbent} = C_{p,s} \cdot m_s \cdot \Delta T \tag{2.27}$$

In the reference paper, steam is used as purge gas, because this is easily condensed afterwards. This makes storing afterwards easier so it is done this way in this research as well. As mentioned the system is not controlled depending on RH and ambient temperatures, so this purge is constant during desorption. The energy required to create this steam is calculated with:

$$E_{purge} = (C_{p,H_2O} \cdot \Delta T + \Delta h_{vap,H_2O}) \cdot \frac{m_{H_2O}}{m_s} \tag{2.28}$$

Where the temperature difference ΔT is roughly 90°C, the heat of vaporisation of water ($\Delta h_{\text{vap},H_2O}$) is 2260 Jg^{-1} and the specific heat capacity of water is 4.2 $\text{Jg}^{-1}\text{K}^{-1}$. With a purge rate of 1.04 $\text{g}_{\text{st}}\text{min}^{-1}\text{kg}_s^{-1}$ for 30 minutes, this gives a steam requirement ($\frac{m_{H_2O}}{m_s}$) of 0.87 $\text{g}_{\text{st}}\text{kg}_s^{-1}$. Everything combined gives a purge energy requirement of 68.6 kJ kg^{-1}.

All the energy requirements are summarised in Table 2.5. It is used to calculate the energy use per cycle, this is again split into a thermal part in Equation 2.29 and an electric part in Equation 2.30. These represent the energy use per cycle which is set constant at 200 minutes total of which 150 minutes is adsorption time, 10 minutes is heating, then 30 minutes of desorption where the purge is on and after that is 10 minutes of cooling.

Table 2.5: Energy requirements for DAC. Reaction heat requirements scale with the amount of material being adsorbed while the others scale with the sorbent mass, which represents the size of the bed

	Component	Value	Unit
Thermal	$\Delta_r H_{CO_2}$	1.7	MJ·$\text{kg}_{CO_2}^{-1}$
	$\Delta_r H_{H_2O}$	4.4	MJ·$\text{kg}_{H_2O}^{-1}$
	$C_{p,s}$	1.58	kJ·kg_s^{-1}·K^{-1}
	e_{reactor}	41	kJ·kg_s^{-1}
	e_{purge}	68.6	kJ·kg_s^{-1}
Electric	$e_{\text{compression}}$	14	kJ·kg_s^{-1}
	e_{vacuum}	30	kJ·kg_s^{-1}

$$E_{thermal} = (\Delta_r H_{CO_2} \cdot q_{CO_2} + \Delta_r H_{H_2O} \cdot q_{H_2O} + C_{p,s} \cdot \Delta T + e_{reactor} + e_{purge}) \cdot m_s \tag{2.29}$$

$$E_{electrical} = (e_{compression} + e_{vacuum}) \cdot m_s \tag{2.30}$$

Validation

The energy calculation is done by splitting the energy requirements in parts, further discussed in the results in Figure 3.7. In order to compare the energy use, it is however better compare the total energy. The average thermal and electrical energy use for Almeria are respectively 16.5 MJ $\text{kg}_{CO_2}^{-1}$ and 1.34 MJ $\text{kg}_{CO_2}^{-1}$ for the average relative humidity of 0.73. When compared with the thermal energy use from Climeworks, which is reported to be 11.9 MJ $\text{kg}_{CO_2}^{-1}$ [50, 71], this is a third higher. The electrical requirement reported by Climeworks is 1.8-2.6 MJ $\text{kg}_{CO_2}^{-1}$ [50, 71], which is slightly higher.

A geospatial analysis by Sendi et al. [55] estimated a thermal energy requirement for DAC of 10.2 MJ $\text{kg}_{CO_2}^{-1}$, and an electrical requirement of 1.1 MJ $\text{kg}_{CO_2}^{-1}$ for Almeria. The energy requirement from this study is 54% higher. The higher use of thermal energy is probably explained by the high energy needed for the desorption of water, which is responsible for 48% of the energy use in the model of this thesis. The GAB isotherm used for water adsorption used in this thesis adsorbs significantly more water than the isotherm used by Senfi from Young et al. [71]. This is taken into account in the sensitivity analysis of the model in section 3.2.

2.4. Cost Calculations

In order to calculate the levelized cost of removed CO_2 (LCOD), the costs for the DAC system as well as the costs of the CSP system are required. One of the outputs of SAM is the levelized cost of electricity (LCOE), which is determined with the CAPEX and a fixed charge rate (FCR) of 0.0616. An overview of the cost components is given in the latest NREL cost update report for 2018 [63]. These costs estimates are

updated since CSP is a technology that is still improving much over the years. An overview of the cost calculations that are being done outside SAM, is shown in Table 2.6. These values have been corrected for currency and inflation using the Chemical Engineering Plant Cost Index (CEPCI) in Table 2.7. This index represents the average costs of chemical plants, it was indexed to 791.4 in January.

The financial parameters used are an inflation rate of 2.5% per year, a project term debt of 100% of the capital cost, and a nominal debt interest rate of 7%. The lifetime used is different for DAC and CSP, respectively 20 and 30 years. All the CSP installation costs are kept at default. It is interesting to note that all costs scale linearly according to the SAM cost evaluation, except for the tower and receiver of the CSP [62]. They respectively have a cost scaling exponent of 0.0113, which is almost a constant with size variations, and 0.7, which results in a five times more expensive system for a ten times bigger size.

Table 2.6: Cost assumptions overview. CAPEX costs are updated with CEPCI shown in Table 2.7. The CAPEX from Climeworks are taken as default and the literature value is used as a lower bound

Parameter	Value	Unit	Reference
Thermal energy requirement Climeworks E_{th}	1750	$\text{kWh}_\text{t} \cdot \text{ton}^{-1}$	[22]
Electrical energy requirement Climeworks E_e	250	$\text{kWh}_\text{e} \cdot \text{ton}^{-1}$	[22]
CAPEX Climeworks	3640	$€{\cdot}\text{ton}^{-1} \cdot \text{yr}^{-1}$	[60]
CAPEX DAC literature	950	$€{\cdot}\text{ton}^{-1} \cdot \text{yr}^{-1}$	[22]
OPEX	4	$\%_{CAPEX} \cdot \text{yr}^{-1}$	[22]
Lifetime DAC	20	yr	[22]
FCR DAC	0.078	–	–
Lifetime CSP	30	yr	[33]
FCR CSP	0.062	–	–
CAPEX Power Cycle	1220	$\$\ \text{kW}_\text{e}^{-1}$	[62]
OPEX CSP	55	$€\ \text{kW}_\text{e}^{-1}{\cdot}\text{yr}^{-1}$	[40]
Electricity use CSP	1–2%	$\text{kWh}_\text{e}{\cdot}\text{kWh}_\text{t}^{-1}$	–
Power cycle efficiency	41.2	%	[62]
Dollar to euro rate	0.90	€/$	–

Table 2.7: Cost assumptions overview, updated to recent value of CEPCI of 795

	Original Value	Reference	Base Year	CEPCI	$ to € [21]	Updated Value
CAPEX Climeworks	€ 3750 $\text{ton}^{-1} \cdot \text{yr}^{-1}$	[60]	2022	816	–	€ 3640 $\text{ton}^{-1} \cdot \text{yr}^{-1}$
CAPEX DAC	€ 730 $\text{ton}^{-1} \cdot \text{yr}^{-1}$	[22]	2019	607.5	–	€ 950 $\text{ton}^{-1} \cdot \text{yr}^{-1}$
CAPEX Power Cycle	\$1040 kW_e^{-1}	[62]	2020	596.2	0.88	€ 1220 kW_e^{-1}

2.4.1. Thermal Energy Storage

One component that largely influences the optimum storage result is the costs of thermal energy storage, which is different for PTC and SPT systems. Since both types generate supply temperatures and use different HTF's with different properties, this differs significantly. According to the SAM standard values, PTC storage costs \$ 62 kWh_t^{-1} while SPT costs just \$ 22 kWh_t^{-1}. An validation overview of the differences is made in Table 2.8. The solar salt used is 60% $NaNO_3$ 40% KNO_3. It should be noted that reliable cost data for all components are scarce, since suppliers often do not publish prices, and academic studies often lack a detailed cost breakdown.

The cost of the heat storage tank is based on a cost breakdown of SPT in which the tank combined with the insulation and all costs associated with it were approximately 50% of the total costs. For PTC systems this is slightly lower because of the lower temperatures and less corrosion, which makes it possible to use cheaper carbon steel instead of stainless steel. The heat exchanger costs are based on a 2017 case study of a PTC plant [23], where it was € 5.2 million for a 50 MW_e plant.

This translates to a plant of 125 MW_t assuming a power cycle efficiency of 37.5% for PTC and 41.5% for SPT due to the higher supplied temperatures [59]. The amount of this cost per kWh_t storage capacity depends on the storage size. In Figure 2.8 the dependency on the storage size of the cost is shown. For 5 hours of storage the costs are roughly € 8 kWh^{-1}, quickly decreasing to less than € 1 kWh^{-1} after 40 hours of storage.

Table 2.8: Calculated cost breakdown of the thermal energy storage for validation. SPT plants have a more than 2 times lower TES cost compared to solar salt storage in PTC, which is in line with the SAM default values

Property	**SPT**	**PTC**	**PTC**	**Unit**	**Reference**
Storage Medium	Solar Salt	Therminol VP-1	Solar Salt	–	–
Temperature	280–500	150–380	280–380	°C	[41]
Density	1800	910	1800	$kg \cdot m^{-3}$	[41]
Specific Heat Capacity	1520	2050	1520	$J \cdot kg^{-1} \cdot K^{-1}$	[62]
HTF Cost	1	25	1	$€ \cdot kg^{-1}$	[62, 6]
Heat Storage Tank Cost	1600	1400	1600	$€ \cdot m^{-3}$	[45]
Heat Exchanger Cost	–	–	42	$€ \cdot kW_t^{-1}$	[23]
Mass Required	10.8	7.6	23.7	$kg \cdot kWh_t^{-1}$	–
Volume Required	6.0×10^{-3}	8.4×10^{-3}	15.6×10^{-3}	$m^3 \cdot kWh_t^{-1}$	–
Total HTF Cost	10.8	190	23.7	$€ \cdot kWh_t^{-1}$	–
Total Tank Cost	9.6	11.8	25.0	$€ \cdot kWh_t^{-1}$	–
Thermal Energy Storage Cost	**20.4**	**201.8**	**48.7**	$\mathbf{€ \cdot kWh_t^{-1}}$	–

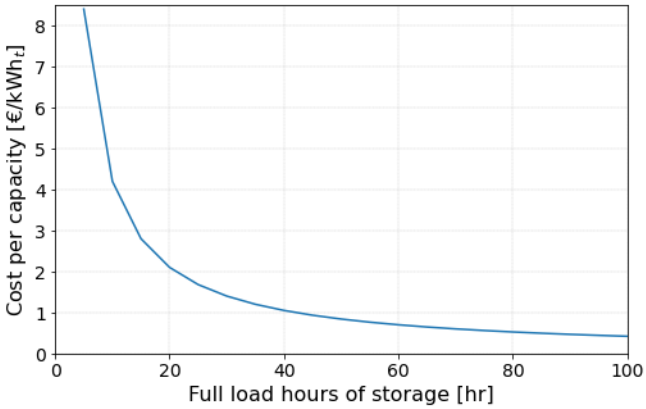

Figure 2.8: Heat exchanger costs depending on storage size

It is clear that storing for PTC becomes expensive when using Therminol due to its high material cost, so a heat exchanger with a molten salt storage is the more interesting option. This option has a small temperature difference due to the maximum temperature being limited by the HTF Therminol to avoid freezing, and the minimum temperature that is determined by the high freezing point of the solar salt. The final cost in this table does not represent a more reliable estimate than SAM, but it gives insight into the factors that determine the large cost difference, which seems valid.

3

Results

3.1. Sizing CSP

The optimal system configuration is determined as the one with the lowest LCOD. This optimum is identified by changing the solar multiple and the hours of storage, and can be explained by analysing the LCOH and capacity. Figure 3.1 shows the LCOH (A, B), capacity (C, D), and LCOD (E, F) with the configuration with PTC on the left and SPT on the right. The results are plotted as a function of solar multiple and storage size, for the typical meteorological year for Almeria. For the PTC system, the optimal LCOH of € 25 MWh^{-1} is achieved with 1 hour of storage and a solar multiple of 1, where the SPT-setup has a LCOH of € 30 MWh^{-1} at the same configuration, indicating that a PTC system without storage gives a higher LCOH than a SPT system. Increasing the solar multiple and hours of storage, raises the LCOH in both systems, but this effect is stronger for PTC. This increase is most notably when increasing the hours of storage, which can be explained by the high TES costs for PTC systems.

The capacity profiles of both systems follow a similar trend, but the SPT system achieves higher capacity for the same amount of SM and HS. At solar multiples close to 1, the capacity does not increase when adding more hours of storage, because there is not enough heat to charge the thermal storage, resulting in the vertical lines on the left. A similar effect is seen around 1 hours of storage, where increasing the solar multiple above a small value will not improve the capacity, but it will even decrease the capacity of the PTC system due to higher losses. Although capacity increases with higher SM and HS, these improvements also lead to higher LCOH.

The optimum for LCOD has the same configuration as the capacity optimum for the SPT system, but the PTC system is limited by the rising LCOH at large storage sizes. The lowest LCOD for a PTC system of € 880 $ton_{CO_2}^{-1}$ can be obtained with a SM of 5.9 and 20 hours of storage, giving a LCOH of € 49 MWh^{-1} with a capacity factor of 0.71. For the SPT configuration, the lowest possible LCOD of € 780 $ton_{CO_2}^{-1}$ is obtained at a SM of 4.8 and 43 hours of storage, which gives a LCOH of € 43 MWh^{-1} with a capacity factor of 0.80. These results indicate that the SPT combination performs better in combination with DAC, especially because of its lower TES cost, which enables higher capacities at lower costs. It should be noted that for smaller installations the PTC configuration might have an advantage because SPT benefits more of economies of scale, discussed in section 2.4.

The CO_2 capture capacity used in Figure 3.1 was obtained by multiplying the maximum DAC capacity with the yearly-averaged capacity factor of the CSP plant. In a more detailed analysis, the energy availably and demand were compared on an hourly basis for the two optimal configurations. This resulted in an optimal PTC system with a true capacity of 74% and an LCOD of € 840 $ton_{CO_2}^{-1}$. The SPT system has a capacity of 82% , this results in a LCOD of € 760 $ton_{CO_2}^{-1}$. Both capacities are slightly higher when matched with their hourly energy demands, this shows that energy efficient DAC weather conditions often occur at the same time as high irradiance. This is expected, since the temperature drops at nights, resulting in higher relative humidity due to lower saturation pressures, which increases the energy demand for DAC. This relation can be clearly seen in Figure 3.2, where the thermal energy requirement of the DAC system is

plotted versus the radiation over six days. The peeks of DNI align with the troughs of DAC energy demand, meaning that the CSP system delivers most heat exactly when DAC requires the least energy per ton CO_2. This increases the potential CO_2 capture rate, meaning that the CSP system delivers most heat exactly when DAC requires the least, which has a positive effect on the potential CO_2 capture rate.

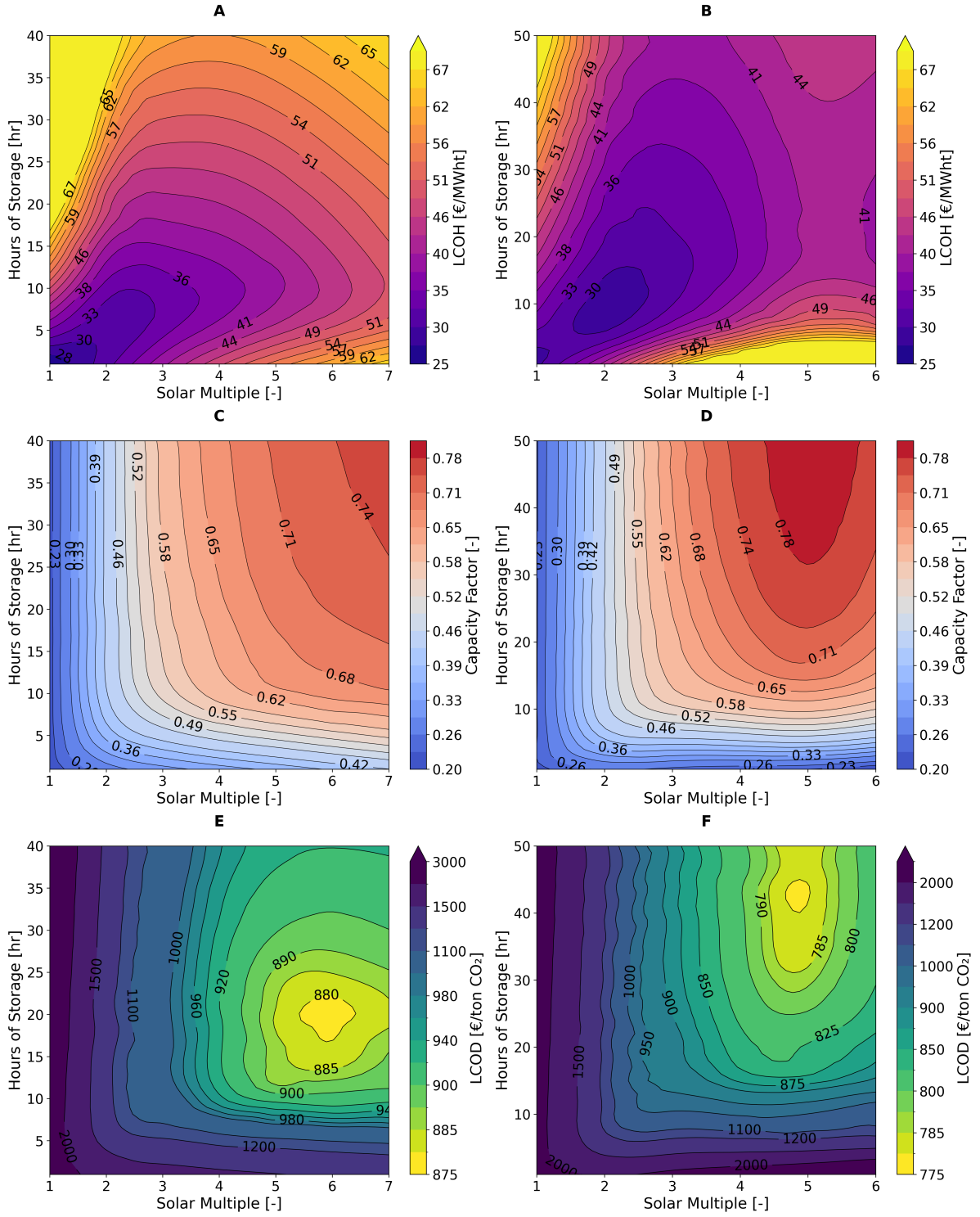

Figure 3.1: On the left side the PTC installation results are shown and at the right side the SPT installation as a function of solar multiple and storage size. From top to bottom are the result for the LCOH (A,B) and capacity (C,D), which are the two determining factors for the LCOD, shown in E and F. It is calculated at intervals of 5 hours of storage and 1 solar multiple, and based on the average values obtained from SAM

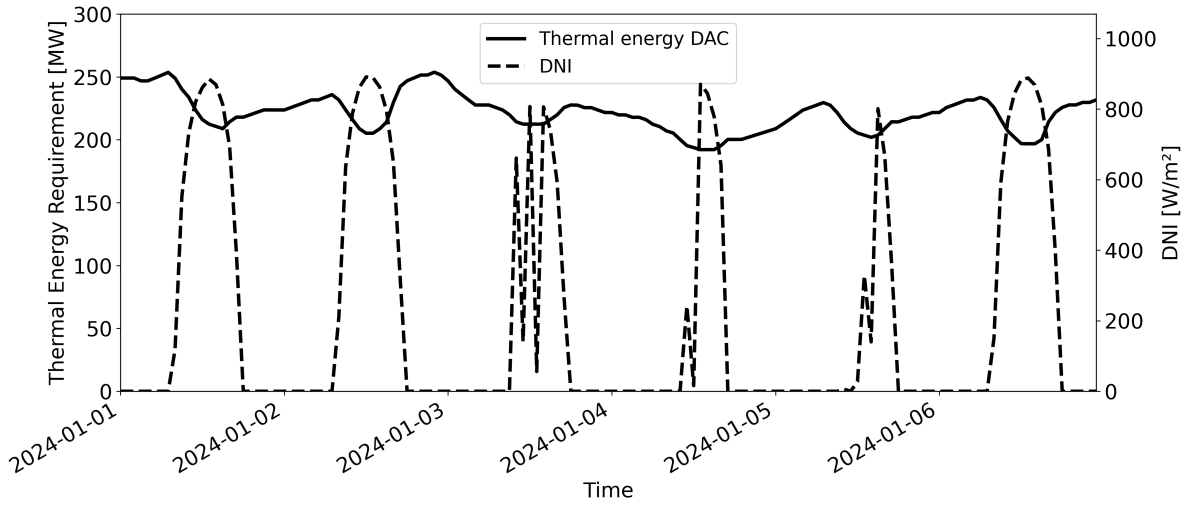

Figure 3.2: The DNI and thermal energy requirement of the DAC system are plotted for the first six days of the typical meteorological year for Almeria. The peaks of DNI align very well with the troughs of the energy requirement. This indicates that the CSP system delivers most heat exactly when DAC requires the least energy per ton CO_2. This effect explains the lower capacity found using average yearly values compared to hourly values

3.2. Cost Sensitivity Analysis

For several components, cost assumptions had to be made due to a lack of reliable real-world reference data. These assumptions have significant uncertainties. To better understand the uncertainties of the LCOD for the base scenario, the cost breakdown of the PTC (A) and SPT (B) systems is shown in Figure 3.3. Both systems have a similar cost distribution, but the biggest difference can be seen in the TES CAPEX. This share is higher for the PTC system, even though it only has 20 hours of storage, compared to 43 hours for the SPT system. The cost breakdown shows that the DAC costs are responsible for a majority of the cost of the system. This is expected because it is still in a relatively low technology readiness level. When the technology matures, the DAC CAPEX and OPEX are expected to drop significantly. In this model the OPEX of DAC are also very significant, since it is defined as a percentage of the CAPEX.

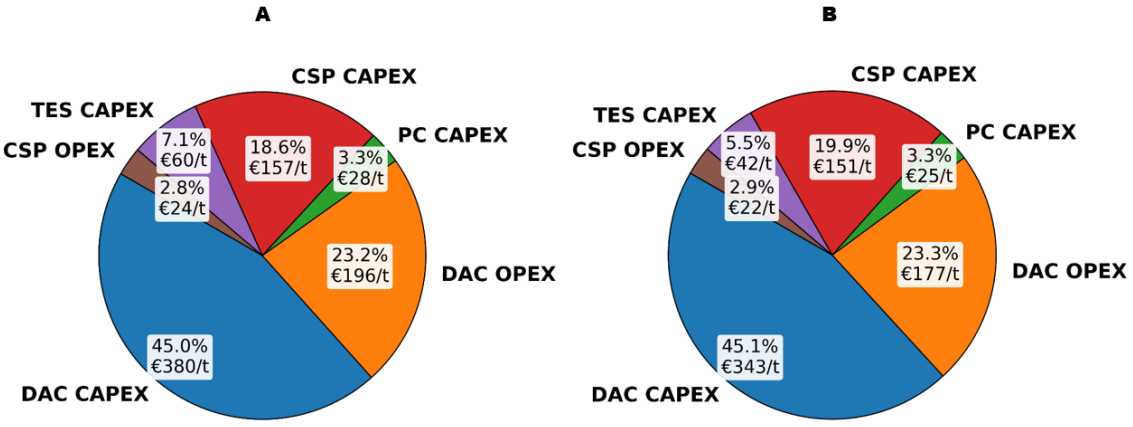

Figure 3.3: The cost breakdown of the S-DAC PTC (A) and SPT (B) combination are very similar, the difference is mainly the total costs. The largest contribution comes from the CAPEX costs of DAC combined with the high OPEX. PC stands for the power cycle costs to generate the electricity

Besides the uncertainty in the DAC CAPEX, the other main sources of uncertainty are: the thermal energy storage CAPEX and the CSP CAPEX, summarised in Table 3.1. These uncertainties result in uncertainties in the LCOD, which can be seen in the normalised sensitivity analysis in Figure 3.4. When the uncertainty is expressed in euros, the uncertainty is larger for PTC due to its higher LCOD. There are small variations for the PTC and SPT system based on the share of the analysed cost factor of the total LCOD. Only for

TES and CSP costs are the differences determined by different cost ranges for the different systems.

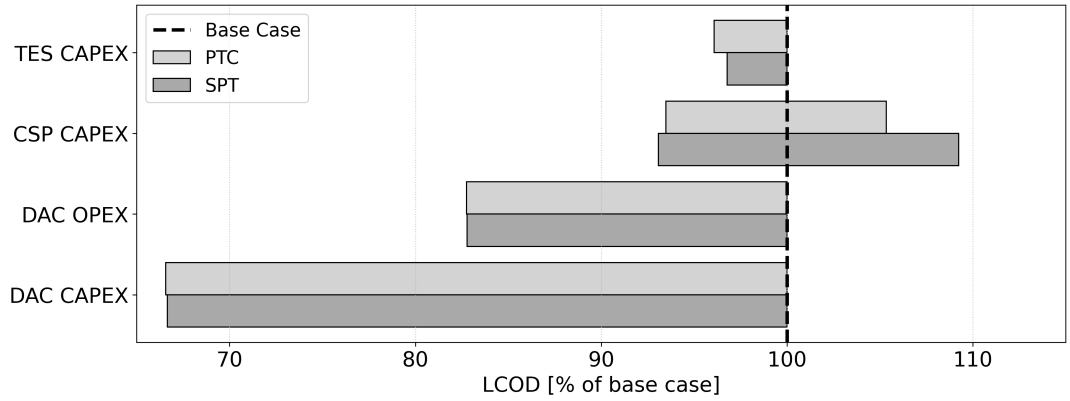

Figure 3.4: Sensitivity analysis on main cost determining factors.

The CSP costs have uncertainty due to variations in CSP costs as well as energy use variations, especially for the amount of water adsorbed. The IEA reports that LCOH of € 27-63 MWh^{-1} are currently successfully being implemented [25], which is in line with the values in Figure 3.1 A and B. The costs for the PTC and SPT systems of respectively € 49 and € 43 MWh^{-1} found here, is in this range but slightly on the lower side, taking into account the large solar multiple and amount of hours of storage. The costs are possibly optimistic and can be respectively 29 and 47% higher for the PTC and SPT system. The CAPEX cost of CSP will also be lower for a lower energy demand, which could realistically go down from 19.8 to 12.9 MJ $kg_{CO_2}^{-1}$. Here the electrical energy is converted to a thermal energy use with the power cycle efficiency, with data obtained from the geospatial DAC analysis from Sendi et al. for Almeria [55].

Reducing the CAPEX costs of DAC will not only drive down the DAC CAPEX, but it will also change the optimal system design. In Figure 3.5 B and D the effect of the change of CAPEX on the selection of the solar multiple and hours of storage is shown for respectively the PTC and SPT system. Lowering the CAPEX costs changes the optimal system configuration for the PTC system only significantly around € 2900 $ton_{CO_2}^{-1}$, mainly by decreasing the hours of storage by 40%, and the configuration remains very constant when decreasing the CAPEX further. A similar instant change can be seen for the SPT system in Figure 3.5 D around € 2700 $ton_{CO_2}^{-1}$, the hours of storage of the TES drops by 25%, while the solar multiple keeps decreasing slightly. The decrease in CSP costs at the corresponding CAPEX value can be seen in figure Figure 3.5 A and B, while this small change is hard to notice, dropping from € 240 at the high CAPEX scenario to € 210 at the low CAPEX scenario for the PTC system and starting at the same for the SPT system, but decreasing to € 220.

It can be concluded that the total CSP costs for the optimal scenario are not significantly influenced by a decrease in DAC CAPEX. The cost breakdown for a scenario with lower CAPEX can therefore be obtained with a high accuracy, from Figure 3.5 A and C. With the lower limit for CAPEX of € 950 $ton_{CO_2}^{-1}$, this gives a LCOD of € 410 for PTC and € 380 for SPT.

Table 3.1: Biggest performance variations that determine the LCOD uncertainty

	Upper limit	**Lower limit**	**Unit**	**Reference**
DAC CAPEX	3640	950	€ $ton^{-1}{\cdot}yr^{-1}$	[60, 22]
Energy use	19.8	12.9	$MJ{\cdot}kg^{-1}$	[71]
LCOH PTC	63	49	€ kWh^{-1}	[33]
LCOH SPT	63	43	€ kWh^{-1}	[33]
TES PTC CAPEX	62	28	€ kWh^{-1}	[62]
TES SPT CAPEX	22	13	€ kWh^{-1}	[62]

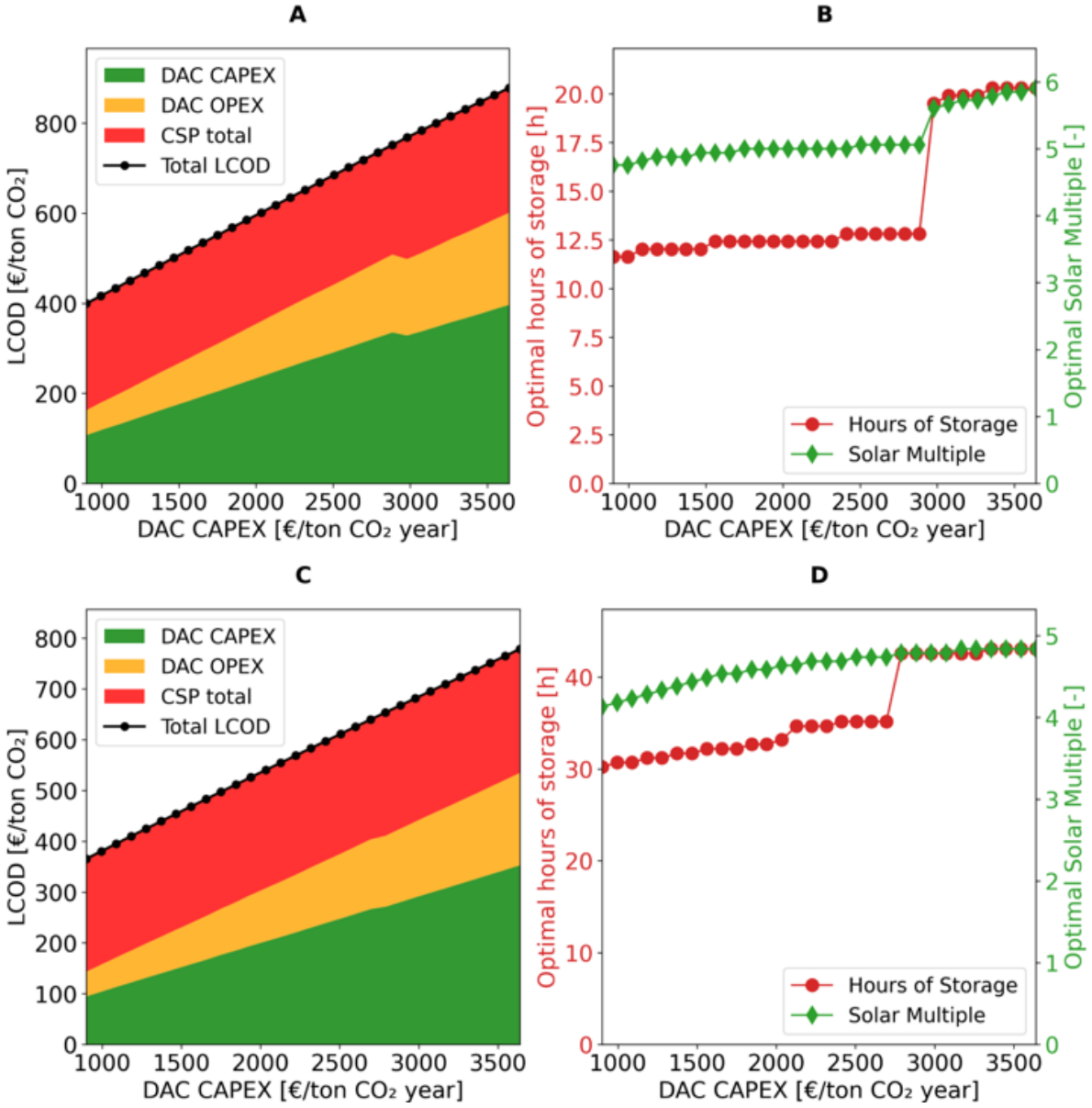

Figure 3.5: Influence on optimal CSP dimensions due to decreasing CAPEX. In figure A, the influence that the decrease in DAC CAPEX cost has on the PTC costs is shown. The whole decrease in Other share LCOD can be attributed to the less expensive optimal PTC configuration. In figure B the selected solar parameters are shown for the changing CAPEX. Figure C and D are the same but for SPT

3.3. Weather Influence

Temperature and humidity both strongly determine the sorbent loading capacity of CO_2 as well as H_2O. In Figure 3.6 A, the effect that temperature and humidity have on the water sorbent loading can be seen for the ranges relevant in Almeria. Increasing humidity always leads to a lower possible CO_2 sorbent loading, but it depends on the humidity if a temperature increase has a positive or negative effect on the possible CO_2 sorbent loading. This is because the equilibrium sorbent loading decreases with temperature, while the kinetics improve with temperature, shown in Figure 2.4.

Relative humidity is very important for desorption, where a higher adsorption humidity leads to more water being adsorbed, visible in Figure 3.6 B. This can significantly worsen the energy requirement, because then the energy is used to desorb water instead of CO_2. In general, increasing relative humidity will worsen system performance, while it depends on humidity if the increase in temperature has a positive or negative effect.

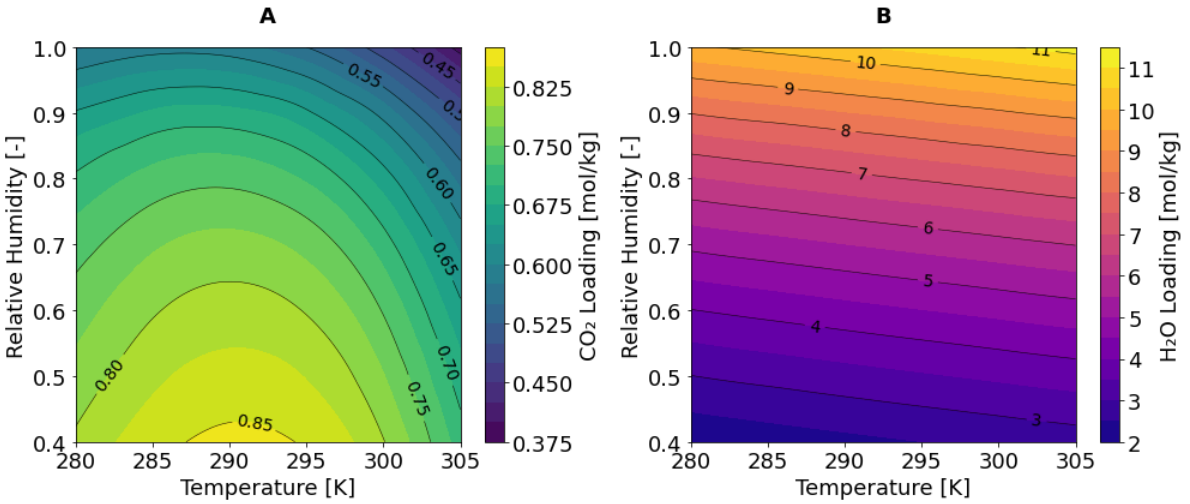

Figure 3.6: Influence of temperature and humidity on A: working capacity of CO_2 and B: working capacity of H_2O with the standard cycle conditions from this thesis

The vastly dryer climate in Alice Springs, Australia, enhances the DAC performance, and the larger more constant irradiance is beneficial for CSP, both weather probability density functions are displayed in Figure 2.6. In Figure 3.7, the thermal energy breakdown for this location (B) is shown besides that of Almeria (A). The required thermal energy per kilogram of CO_2 decreases significantly from 16.5 to 10.9 MJ $kg_{CO_2}^{-1}$, almost entirely due to a lower energy requirement for desorbing water. The electrical energy differs less than 1%.

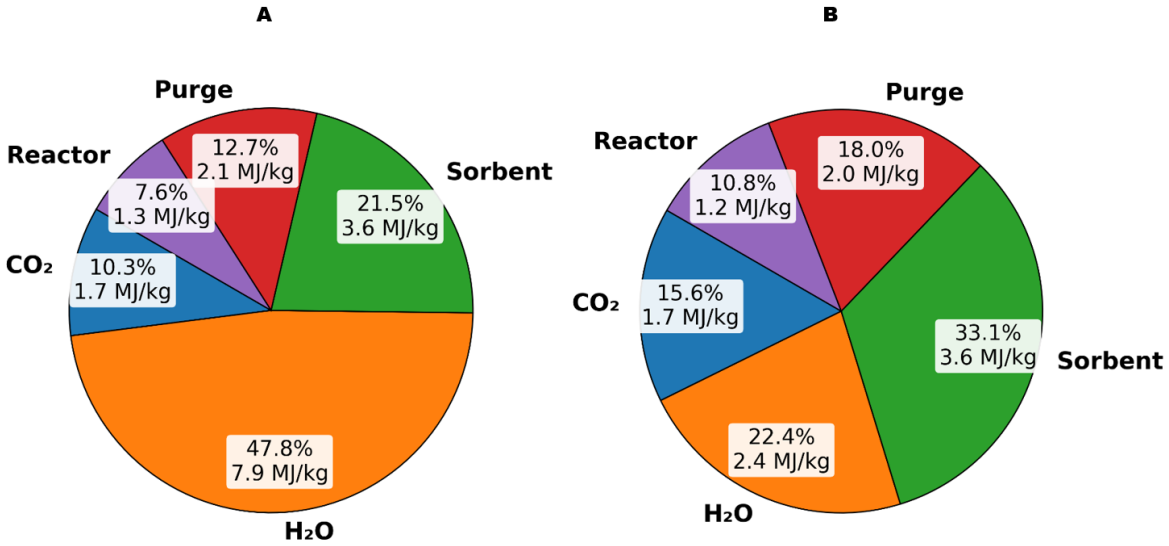

Figure 3.7: Energy breakdown at Almeria (A) and Alice Springs Australia (B). Lower humidities show a significantly lower energy use for H_2O desorption in Alice Springs

With the different energy use and supply, a vastly different optimum scenario is found for Alice Springs. In Figure 3.8 the LCOD is plotted for PTC (A) and SPT (B) systems, similarly to Figure 3.1. The capacity and LCOH are not presented for this location because they show similar patterns compared to Almeria, apart from lower values for LCOH, and higher values for capacity at the same locations. This is the reason that the optimum configuration has shifted to a considerably lower solar multiple and amount of hours of storage.

For PTC the optimum is at a SM of 2.5 and 9 hours of storage, which gives a LCOD of € 650 $ton_{CO_2}^{-1}$, with a LCOH of € 26 MWh^{-1} and a capacity of 84%. For a SPT system with a solar multiple of 2.1 and a storage of

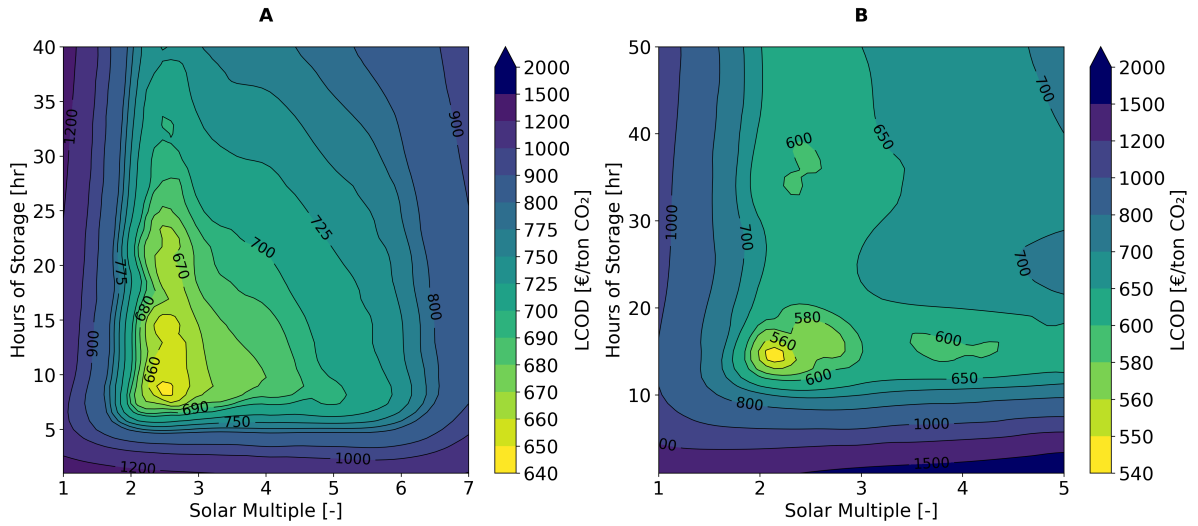

Figure 3.8: Levelized cost of removed CO_2 for the base case high CAPEX scenario in Alice Springs for A: PTC and B: SPT. It is calculated at intervals of 5 hours of storage and 1 solar multiple

14 hours, a LCOD of € 550 $ton_{CO_2}^{-1}$ is obtainable with a LCOH of € 21 MWh^{-1} and a capacity of 92%. When the DAC CAPEX costs are lowered to € 960 $ton_{CO_2}^{-1}$ $year^{-1}$, the optimal configuration changes less than 2% for this location. Compared to Almeria this location has optimums at more than two times smaller solar multiples and 2 and 4 times less hours of storage for PTC and SPT respectively. Both systems are € 200 $ton_{CO_2}^{-1}$ cheaper than the systems in Almeria due to the lower energy requirement combined with the high capacity found at smaller CSP and storage sizes, due to smaller seasonal DNI variations.

3.4. CO_2 Capture per Land Use

Due to the large financial uncertainties, it can be more insightful to express the production per land use or aperture area instead of costs. In Table 3.2 the land use, aperture area and the corresponding yearly capture rate of CO_2 is given for all locations. This is given for the cost optimum configuration (CO) for PTC and SPT, as well as the minimum-area configuration (MA). These values are then used to obtain the lowest cost optimum of the land use per capacity and aperture area per capacity. The minimal area scenario represents a case where all energy from CSP can directly be supplied to the DAC. This is the situation with a solar multiple of one, zero storage and no output constraints, which will be an expensive option due to the low capacity.

For the cost optimum, the PTC system in Alice Springs has the lowest land use per capacity of 10.3 $m^2/(ton_{CO_2}\ yr^{-1})$. This is only 2 $m^2/(ton_{CO_2}\ yr^{-1})$ more than for a minimum area. In terms of land use PTC scores significantly better than SPT systems. The minimum required aperture area is similar for PTC and SPT in Alice Srings. For optimising costs an area of 3.6-3.7 $m^2/(ton_{CO_2}\ yr^{-1})$ is needed while the lowest possible aperture area requirement is 3.0 $m^2/(ton_{CO_2}\ yr^{-1})$. This small difference in optimal land use and aperture area shows that the plants in Alice Springs are able to utilise 81-83% of the heat supplied from the CSP plant, to the DAC system. In Almeria this is only 61-66%.

Taking the inverse of land use per capacity gives the capture rate of CO_2 per year per square meter to

Table 3.2: For the four scenarios, an overview of land use aperture area and production of CO_2 is given for the cost optimum (CO) and minimum area (MA) configuration. Land use and aperture area per capacity are calculated from these values

System	Land use [km^2]		Aperture area [km^2]		Yearly production [10^5 ton_{CO_2} yr^{-1}]		Land use per capacity [$m^2/(ton_{CO_2}\ yr^{-1})$]		Aperture area per capacity [$m^2/(ton_{CO_2}\ yr^{-1})$]	
	CO	**MA**	**CO**	**MA**	**CO**	**MA**	**CO**	**MA**	**CO**	**MA**
PTC Almeria	9.85	1.7	3.58	0.62	3.17	0.9	31.1	18.9	11.3	6.9
SPT Almeria	26.2	4.9	4.13	0.78	3.51	1.0	74.6	49.0	11.8	7.8
PTC Alice Springs	3.97	1.6	1.44	0.57	3.85	1.9	10.3	8.3	3.7	3.0
SPT Alice Springs	9.57	4.2	1.58	0.72	4.21	2.4	22.7	17.5	3.6	3.0

be between 13–97 kg_{CO_2} m_l^2 $year^{-1}$. By contrast, forests capture 0.4–4 kg_{CO_2} m_l^2 $year^{-1}$ [11], depending on the tree type and climate. With the low land use DAC scenario, it has the potential to capture more than 20 times more CO_2 per land area than the best carbon capturing tree and 200 times more than the worst. The land use of the DAC system itself is neglected because this is insignificant compared to the CSP land use [55]. The other advantage of DAC is that it can be placed in locations where not many trees grow due to the high temperatures, like in Australia, while this location does give a high performance for the DAC-CSP combination.

SPT requires roughly 2.3 times more land per ton_{CO_2} $year^{-1}$, while the aperture area is only 10-15% higher per capture capacity. This can be explained by the fact that heliostats have to be spaced so that they do not interfere with other heliostats, while PTC collectors can be placed relatively close to each other. Increasing the size of the SPT plant results in a less efficient land use, because the outer heliostats have to be placed further away from each other, to avoid blocking. In SAM increasing the solar multiple with a factor 4 results in 4.6 times more land use for SPT. This does not explain the whole difference, but according to Alamni et al. [5] SPT installations use 1.4 times as much land as PTC. Together with the fact that the SPT heliostat configuration is optimised for costs and not for land use, this big difference can be explained.

The difference in required aperture and land use per capacity for the same CSP type on a different location, is more than a factor 3 for the cost optimum scenario and slightly lower for the minimal area. This is because of the lower energy use of the location due to lower humidities as well as a higher, more constant solar irradiance, which gives a higher capacity. This resulted in an optimal configuration with a smaller solar multiple for Almeria, reducing its land and aperture area requirement.

3.5. CSP Validation

The solar-to-heat efficiency of both systems, defined as annual heat generation divided by annual direct irradiance on aperture, is 51% for PTC and 41% for SPT installations. In literature solar-to-electricity ranges between 12-16% [61] are reported, with values above 16% are obtained as well [5]. With power cycle efficiency of 40% this higher value becomes 40% solar-to-heat efficiency.

This is in line with the found 41% efficiency for SPT. Optical efficiency of the used SkyThrough collector is reported to be around 80% and thermal efficiency in the loop is dependent on DNI and temperature, and is roughly 80% for the conditions used in the article from Jing-hu et al. [29]. This results in a total efficiency of 64%, so the plant designed in this thesis is 20% less efficient with a total efficiency of 51%. This 64% seems to be on the high side however, but the extra loss factor can be contributed to the efficiency of the TES.

In another study done on a SPT installation, the collector efficiency is said to be 75%, parasitic efficiency 88% and the receiver efficiency 90% [70], resulting in a solar-to-heat efficiency of 59%, where the majority of losses come from the heliostat field. This reported efficiency is also on the high side, but it gives the best insight into the part with the highest losses. It reports a solar-to-electricity efficiency of 23% which is really high compared to the previous mentioned 12-16%. Efficiencies of CSP plants are not being reported very often, but with the found efficiencies the CSP systems seem to be performing between the low and high efficiency found from the literature.

4

Conclusion

This thesis investigates the techno-economic performance of integrating solid sorbent direct air capture (S-DAC) with concentrated solar power (CSP). Two CSP technologies are analysed: parabolic trough collectors (PTC) and solar power towers (SPT). For both CSP types, two high-DNI locations were evaluated: Almeria (Spain), representing a feasible European site, and Alice Springs (Australia), offering superior irradiance. A pseudo-dynamic hourly model, based on the typical meteorological year, is used to evaluate the optimal configuration as well as the performance, cost and land use.

The results show that SPT has the potential to be the solution with the lowest levelised cost of captured CO_2 of € 760 $\text{ton}_{CO_2}^{-1}$ for the base scenario. This requires a solar field with a high solar multiple of 4.8 and 43 hours of storage, which is significantly more than the optimum for levelised cost of heat. It was found that oversizing TES and the solar field beyond the cost-optimal point significantly increases DAC uptime, which is required to spread the high CAPEX of the DAC system over more tonnes captured.

The cost share of DAC is 68% for both DAC-CSP systems, this cost is also the dominant source of uncertainty according to the sensitivity analysis. The sensitivity analysis shows that lowering DAC CAPEX does not significantly affect the CSP system cost. As a result, the LCOD can be estimated with high accuracy in scenarios with lower DAC costs. With the low scenario DAC CAPEX of € 960 $\text{ton}_{CO_2}^{-1}$ yr^{-1}, the LCOD drops to € 410 $\text{ton}_{CO_2}^{-1}$ for PTC and € 380 for SPT. This is below € 600 $\text{ton}_{CO_2}^{-1}$, realised by Climeworks' [17], where geothermal energy is being used. Pairing DAC with small modular nuclear reactors is reported to have LCOD of € 250 $\text{ton}_{CO_2}^{-1}$, assuming DAC CAPEX of € 1226 $\text{ton}_{CO_2}^{-1}$ yr^{-1}. This might be optimistic, as geothermal heat in Iceland is likely very cheap, and nuclear LCOD is twice as low.

The location plays a major role in the performance of the combination. A high and constant DNI is required for a large constant supply of heat and a low relative humidity is required for a lower energy use during desorption. This combination is found in Alice Springs Australia, and it is found to bring down LCOD by 23 and 27% for respectively PTC and SPT compared to Almeria. This is partly due to a 30% lower energy requirement and partly due to the near 50% reduction of LCOH.

From a land-use perspective, SPT systems did not outperform PTC which requires 2.3 times less land in the optimal cost scenario. Notably, the combination captures more than 20 times as much CO_2 per square meter than the most efficient carbon-capturing trees, with the added benefit of being usable in regions unsuitable for forestry. In Almeria, the cost-optimal solution requires up to 60% more aperture area for PTC than the area-optimal configuration, highlighting trade-offs between cost and land efficiency.

In summary, the combination of DAC with SPT is the most cost efficient solution, while the PTC configuration required significantly less land. For smaller installations, PTC might be more economical. The best-performing setup can capture over 20 times as much CO_2 per square meter as the most efficient trees in ideal conditions. Combining CSP with DAC is technically feasible and has the most potential in regions with high solar irradiance and low relative humidity. CSP provides a scalable heat source, that can be located in more locations than the cheap geothermal solution, and faces less public resistance than nuclear energy, while achieving comparable costs.

5

Recommendations

Many sources suggested that the adsorption of CO_2 is influenced by the relative humidity [50, 16]. The effect that humidity has on the energy demand due to water adsorption is not taken into account, but the effect that H_2O has on CO_2 adsorption is not taken into account. Two different methods can be used to add this effect. The easiest to implement method would be to change the temperature to an empirical equivalent adsorption temperature that takes RH into account, discussed by Sabatino et al. [50]. High humidity decreases the equivalent adsorption temperature, which leads to slower kinetics, but a higher equilibrium CO_2 sorbent loading. The other method would be to change the CO_2 isotherm to the weighted average dual-site Toth model, which takes into account RH [15].

Replacing the fixed bed with a moving bed could significantly reduce the energy losses. Although most studies are now focussed on fixed beds, moving beds are expected to have a lower energy consumption. Creating accessible information, especially about the costs of moving beds as well as the probably lower energy requirements, would help to get better cost estimations.

The combination of DAC and CSP has never been tested on a realistic scale, to the authors best knowledge. Building a first-of-its-kind combined installation to obtain real performances, would be very helpful for realistic insights. This should ideally be done with the optimal SPT configuration, but a PTC system could be a smaller early-stage test site. Building this at the two suggested locations will also be possible this way, which will give more insight into the performance at different climates.

In the test site, measuring temperatures to obtain the heat transfer coefficient and desorption heat kinetics could give more insight into the process. Potentially the relatively low temperature supplied from the TES for the PTC system can be limiting heat transfer. The higher supplied temperatures obtained in the SPT system on the other hand, might increase the desorption rate significantly. Integrating the heat has not been fully thought through, but this can reduce the energy requirement of heating the sorbent, reactor and purge significantly. Measuring the desorption kinetics and capture rates can help to optimise the process further, reducing the LCOD.

The last thing that would be interesting to add to this research would be to utilise a similar strategy as Prats-Salvado et al. [48]. They designed a system where CO_2 is almost constantly adsorbed, since this requires a relatively small amount of energy, and it is being desorbed when there is sufficient thermal energy available. This will only work with a moving bed, and a significantly larger desorption unit. To evaluate this method can be a challenge because realistic prices of the components are required to know if it will lower the cost more than adding thermal energy storage does.

Some improvements for the model used are suggested, but what can be more interesting is designing a fully integrated process model. This way control strategies can be optimised and real performance can be obtained. Testing such a plant in different weather conditions can validate the findings from this research.

References

[1] National Renewable Energy Laboratory (NREL). *SAM Case Study: Andasol-1*. Tech. rep. Accessed June 2025. National Renewable Energy Laboratory (NREL), 2013.

[2] National Renewable Energy Laboratory (NREL). *SAM Case Study: Gemasolar*. Tech. rep. Accessed June 2025. National Renewable Energy Laboratory (NREL), 2013.

[3] International Energy Agency. *CO2 Emissions*. 2024. URL: https://www.iea.org/reports/global-energy-review-2025/co2-emissions (visited on 06/24/2025).

[4] International Energy Agency. *Tracking Clean Energy Progress 2023*. 2024. URL: https://www.iea.org/reports/tracking-clean-energy-progress-2023 (visited on 10/15/2024).

[5] Abdul Hai Alami et al. "Concentrating solar power (CSP) technologies: Status and analysis". In: *International Journal of Thermofluids* 18 (May 2023). ISSN: 26662027. DOI: 10.1016/j.ijft.2023.100340.

[6] Guruprasad Alva, Yaxue Lin, and Guiyin Fang. "An overview of thermal energy storage systems". In: *Energy* 144 (Feb. 2018), pp. 341–378. ISSN: 03605442. DOI: 10.1016/j.energy.2017.12.037.

[7] Keju An et al. "Direct air capture with amino acid solvent: Operational optimization using a crossflow air-liquid contactor". In: *AIChE Journal* 70 (9 Sept. 2024). ISSN: 15475905. DOI: 10.1002/aic.18429.

[8] Deborah Ayres and Lourdes Zamora. *Renewable Power Generation Costs in 2023*. Tech. rep. International Renewable Energy Agency (IRENA), 2024.

[9] Cyril Jose E. Bajamundi et al. "Capturing CO2 from air: Technical performance and process control improvement". In: *Journal of CO2 Utilization* 30 (Mar. 2019), pp. 232–239. ISSN: 22129820. DOI: 10.1016/j.jcou.2019.02.002.

[10] Candelaria Bergero et al. "Pathways to net-zero emissions from aviation". In: *Nature Sustainability 2023 6:4* 6 (4 Jan. 2023), pp. 404–414. ISSN: 2398-9629. DOI: 10.1038/s41893-022-01046-9.

[11] Blanca Bernal, Lara T. Murray, and Timothy R. H. Pearson. "Global carbon dioxide removal rates from forest landscape restoration activities". In: *Carbon Balance and Management* 13.1 (2018), p. 22. ISSN: 1750-0680. DOI: 10.1186/s13021-018-0110-8.

[12] Luca Bertoni et al. "Integrating direct air capture with small modular nuclear reactors: understanding performance, cost, and potential". In: *JPhys Energy* 6 (2 Apr. 2024). ISSN: 25157655. DOI: 10.1088/2515-7655/ad2374.

[13] Bloomberg. *EU ETS Market Outlook 1H 2024: Prices Valley Before Rally*. Accessed: 2024-10-15. 2024. URL: https://about.bnef.com/insights/commodities/eu-ets-market-outlook-1h-2024-prices-valley-before-rally/.

[14] Alberto Boretti, Jamal Nayfeh, and Wael Al-Kouz. "Validation of SAM Modeling of Concentrated Solar Power Plants". In: *Energies* 13.8 (2020). ISSN: 1996-1073. DOI: 10.3390/en13081949.

[15] Florian M. Chimani et al. "Evaluation of CO2/H2O Co-Adsorption Models for the Anion Exchange Resin Lewatit VPOC 1065 under Direct Air Capture Conditions Using a Novel Lab Setup". In: *Separations* 11 (6 June 2024). ISSN: 22978739. DOI: 10.3390/separations11060160.

[16] Florian Maximilian Chimani. "Experimental evaluation of an adsorbent under direct air capture conditions". MA thesis. TU Wien, 2022. DOI: https://doi.org/10.34726/hss.2022.92425.

[17] Climeworks. *Next generation tech powers Climeworks' megaton leap*. 2024. URL: https://climeworks.com/press-release/next-gen-tech-powers-climeworks-megaton-leap (visited on 10/15/2024).

[18] Alexander W. Dowling, Tian Zheng, and Victor M. Zavala. "Economic assessment of concentrated solar power technologies: A review". In: *Renewable and Sustainable Energy Reviews* 72 (2017), pp. 1019–1032. ISSN: 1364-0321. DOI: doi.org/10.1016/j.rser.2017.01.006.

[19] Rick T. Driessen, Sascha R.A. Kersten, and Derk W.F. Brilman. "A Thiele Modulus Approach for Nonequilibrium Adsorption Processes and Its Application to CO2 Capture". In: *Industrial and Engineering Chemistry Research* 59 (15 Apr. 2020), pp. 6874–6885. ISSN: 15205045. DOI: 10.1021/acs.iecr.9b05503.

[20] Jere Elfving and Tuomo Sainio. "Kinetic approach to modelling CO2 adsorption from humid air using amine-functionalized resin: Equilibrium isotherms and column dynamics". In: *Chemical Engineering Science* 246 (2021), p. 116885. ISSN: 0009-2509. DOI: https://doi.org/10.1016/j.ces.2021.116885.

[21] Eurostat. *Exchange rates and interest rates*. https://ec.europa.eu/eurostat/statistics-explained/index.php?title=Exchange_rates_and_interest_rates&oldid=664154. Data extracted in January 2025. 2025.

[22] Mahdi Fasihi, Olga Efimova, and Christian Breyer. "Techno-economic assessment of CO2 direct air capture plants". In: *Journal of Cleaner Production* 224 (2019), pp. 957–980. ISSN: 0959-6526. DOI: https://doi.org/10.1016/j.jclepro.2019.03.086.

[23] P. A. González-Gómez et al. "Cost-based design optimization of the heat exchangers in a parabolic trough power plant". In: *Energy* 123 (2017), pp. 314–325. ISSN: 03605442. DOI: 10.1016/j.energy.2017.02.002.

[24] Waleed M. Hamanah et al. "Solar Power Tower Drives: A Comprehensive Survey". In: *IEEE Access* 11 (2023), pp. 83964–83982. ISSN: 21693536. DOI: 10.1109/ACCESS.2021.3066799.

[25] IEA SHC Task 64 / SolarPACES Task IV Working Group. *Technology Position Paper on Solar Heat for Industrial Processes (SHIP)*. https://www.iea-shc.org/Data/Sites/1/publications/IEA-SHC-Task64-Technology-Position-Paper-SHIP-2024-01.pdf. IEA Solar Heating and Cooling Programme, Task 64 / SolarPACES Task IV. Jan. 2024.

[26] IPCC. *Climate Change 2022: Mitigation of Climate Change. Contribution of Working Group III to the Sixth Assessment Report of the Intergovernmental Panel on Climate Change*. Ed. by P.R. Shukla et al. Cambridge, UK and New York, NY, USA: Cambridge University Press, 2022. Chap. 12.3. DOI: 10.1017/9781009157926.

[27] IPCC. *Global Warming of 1.5°C: Strengthening and Implementing the Global Response*. Ed. by Heleen de Coninck et al. Cambridge, UK and New York, NY, USA: Cambridge University Press, 2018. Chap. 4. DOI: 10.1017/9781009157940.006.

[28] Md Tasbirul Islam et al. "A comprehensive review of state-of-the-art concentrating solar power (CSP) technologies: Current status and research trends". In: *Renewable and Sustainable Energy Reviews* 91 (Aug. 2018), pp. 987–1018. ISSN: 18790690. DOI: 10.1016/j.rser.2018.04.097.

[29] Gong Jing-hu et al. "Performance optimization of larger-aperture parabolic trough concentrator solar power station using multi-stage heating technology". In: *Energy* 268 (2023), p. 126640. ISSN: 0360-5442. DOI: https://doi.org/10.1016/j.energy.2023.126640.

[30] Christopher W. Jones. "CO(2) capture from dilute gases as a component of modern global carbon management." In: *Annual Review of Chemical and Biomolecular Engineering* 2 (Jan. 2011), pp. 31–52. ISSN: 1947-5438. DOI: 10.1146/ANNUREV-CHEMBIOENG-061010-114252.

[31] David W. Keith et al. "A Process for Capturing CO2 from the Atmosphere". In: *Joule* 2 (8 Aug. 2018), pp. 1573–1594. ISSN: 25424351. DOI: 10.1016/j.joule.2018.05.006.

[32] Devon Kesseli et al. "CSP-plant modeling guidelines and compliance of the system advisor model (SAM)". In: *AIP Conference Proceedings* 2126.1 (July 2019), p. 170006.

[33] Muhammad Imran Khan et al. "The economics of concentrating solar power (CSP): Assessing cost competitiveness and deployment potential". In: *Renewable and Sustainable Energy Reviews* 200 (Aug. 2024). ISSN: 18790690. DOI: 10.1016/j.rser.2024.114551.

[34] Shuangjun Li et al. "Solar thermal energy-assisted direct capture of CO2 from ambient air for methanol synthesis". In: *npj Materials Sustainability* 2 (1 May 2024). DOI: 10.1038/s44296-024-00014-y.

[35] May-Yin Ashlyn Low et al. "Measurement of Physicochemical Properties and CO2, N2, Ar, O2, and H2O Unary Adsorption Isotherms of Purolite A110 and Lewatit VP OC 1065 for Application in Direct Air Capture". In: *Journal of Chemical & Engineering Data* 68.12 (2023), pp. 3499–3511. DOI: 10.1021/acs.jced.3c00401.

[36] Alex Marcil et al. “Experimentation of a Novel Sequential Moving Bed DAC System”. In: *17th International Conference on Greenhouse Gas Control Technologies, GHGT-17*. 2024.

[37] Noah McQueen et al. “A review of direct air capture (DAC): Scaling up commercial technologies and innovating for the future”. In: *Progress in Energy* 3 (3 July 2021). ISSN: 25161083. DOI: 10.1088/2516-1083/abf1ce.

[38] Noah McQueen et al. “Cost Analysis of Direct Air Capture and Sequestration Coupled to Low-Carbon Thermal Energy in the United States”. In: *Environmental Science and Technology* 54 (12 June 2020), pp. 7542–7551. ISSN: 15205851. DOI: 10.1021/acs.est.0c00476.

[39] Hasan Muslemani et al. “Opportunities and challenges for decarbonizing steel production by creating markets for ‘green steel’ products”. In: *Journal of Cleaner Production* 315 (2021), p. 128127. ISSN: 0959-6526. DOI: https://doi.org/10.1016/j.jclepro.2021.128127.

[40] National Renewable Energy Laboratory. *2024 Annual Technology Baseline: Concentrating Solar Power*. https://atb.nrel.gov/electricity/2024/concentrating_solar_power. Accessed on April 28, 2025. 2024.

[41] National Renewable Energy Laboratory (NREL). *System Advisor Model (SAM) Version 2022.11.21*. https://sam.nrel.gov. Computer software, Golden, CO. 2022.

[42] Michele Negri et al. “New technologies for ammonium dinitramide based monopropellant thrusters – The project RHEFORM”. In: *Acta Astronautica* 143 (Nov. 2017). DOI: 10.1016/j.actaastro.2017.11.016.

[43] Takeshi Okumura et al. “Modeling of moving bed CO2 capture process using amine solid adsorbent and its validation using pilot plant test data”. In: *International Journal of Greenhouse Gas Control* 133 (2024), p. 104094. ISSN: 1750-5836. DOI: https://doi.org/10.1016/j.ijggc.2024.104094.

[44] Sean Ong et al. *Land-Use Requirements for Solar Power Plants in the United States*. 2013.

[45] Laura Pompei, Fabio Nardecchia, and Adio Miliozzi. “Current, Projected Performance and Costs of Thermal Energy Storage”. In: *Processes* 11 (3 Mar. 2023). ISSN: 22279717. DOI: 10.3390/pr11030729.

[46] Enric Prats-Salvado, Nathalie Monnerie, and Christian Sattler. “Synergies between direct air capture technologies and solar thermochemical cycles in the production of methanol”. In: *Energies* 14 (16 Aug. 2021). ISSN: 19961073. DOI: 10.3390/en14164818.

[47] Enric Prats-Salvado, Nathalie Monnerie, and Christian Sattler. “Techno-Economic Assessment of the Integration of Direct Air Capture and the Production of Solar Fuels”. In: *Energies* 15 (14 July 2022). ISSN: 19961073. DOI: 10.3390/en15145017.

[48] Enric Prats-Salvado et al. “Solar-Powered Direct Air Capture: Techno-Economic and Environmental Assessment”. In: *Environmental Science and Technology* 58 (5 Feb. 2024), pp. 2282–2292. ISSN: 15205851. DOI: 10.1021/acs.est.3c08269.

[49] Hannah Ritchie, Pablo Rosado, and Veronika Samborska. *Carbon dioxide concentrations in the atmosphere*. 2024. URL: https://ourworldindata.org/grapher/co2-long-term-concentration (visited on 10/15/2024).

[50] Francesco Sabatino et al. “A comparative energy and costs assessment and optimization for direct air capture technologies”. In: *Joule* 5 (8 Aug. 2021), pp. 2047–2076. ISSN: 25424351. DOI: 10.1016/j.joule.2021.05.023.

[51] Muhammad Munir Sadiq et al. “Engineered Porous Nanocomposites That Deliver Remarkably Low Carbon Capture Energy Costs”. In: *Cell Reports Physical Science* 1 (6 June 2020). ISSN: 26663864. DOI: 10.1016/j.xcrp.2020.100070.

[52] Paula Sophie Sauter. “Mass transfer in Direct Air Capture sorbents - Modeling adsorption and desorption of carbon dioxide and water in typical solid sorbents”. MA thesis. Delft University of Technology, 2024.

[53] H. M. Schellevis and D. W. F. Brilman. “Experimental study of CO2 capture from air via steam-assisted temperature-vacuum swing adsorption with a compact kg-scale pilot unit”. In: *React. Chem. Eng.* 9 (4 2024), pp. 910–924. DOI: 10.1039/D3RE00460K.

[54] H. M. Schellevis, T. N. van Schagen, and D. W.F. Brilman. "Process optimization of a fixed bed reactor system for direct air capture". In: *International Journal of Greenhouse Gas Control* 110 (Sept. 2021). ISSN: 17505836. DOI: 10.1016/j.ijggc.2021.103431.

[55] Marwan Sendi et al. "Geospatial analysis of regional climate impacts to accelerate cost-efficient direct air capture deployment". In: *One Earth* 5 (10 Oct. 2022), pp. 1153–1164. ISSN: 25903322. DOI: 10.1016/j.oneear.2022.09.003.

[56] Xiaoyang Shi, Yuanchunyu Lin, and Xi Chen. "Development of sorbent materials for direct air capture of CO2". In: *MRS Bulletin* 47.4 (2022), pp. 405–415.

[57] Katrin Sievert, Tobias S. Schmidt, and Bjarne Steffen. "Considering technology characteristics to project future costs of direct air capture". In: *Joule* 8 (4 Apr. 2024), pp. 979–999. ISSN: 25424351. DOI: 10.1016/j.joule.2024.02.005.

[58] Valentina Stampi-Bombelli, Mijndert van der Spek, and Marco Mazzotti. "Analysis of direct capture of CO 2 from ambient air via steam-assisted temperature–vacuum swing adsorption". In: *Adsorption* 26 (7 Oct. 2020), pp. 1183–1197. ISSN: 15728757. DOI: 10.1007/s10450-020-00249-w.

[59] W.H. Stein and R. Buck. "Advanced power cycles for concentrated solar power". In: *Solar Energy* 152 (2017). Progress in Solar Energy Special Issue: Concentrating Solar Power (CSP), pp. 91–105. ISSN: 0038-092X. DOI: https://doi.org/10.1016/j.solener.2017.04.054.

[60] The Guardian. *World's biggest plant to turn carbon dioxide into rock opens in Iceland – Orca*. The Guardian (online). Accessed June 2025. Sept. 2021.

[61] Franz Trieb et al. "Global Potential of Concentrating Solar Power". In: *Proceedings of SolarPACES Conference*. Based on data from NASA SSE v6.0; part of the REACCESS project. Berlin, Germany, Sept. 2009.

[62] Craig Turchi et al. *CSP Systems Analysis – Final Project Report*. Tech. rep. NREL/TP-5500-72856. National Renewable Energy Laboratory (NREL), 2019.

[63] Craig S. Turchi et al. *CSP Systems Analysis – Final Project Report*. Tech. rep. NREL/TP-5500-72856. Golden, CO: National Renewable Energy Laboratory, 2019.

[64] Rens Veneman et al. "Adsorption of H2O and CO2 on supported amine sorbents". In: *International Journal of Greenhouse Gas Control* 41 (Oct. 2015), pp. 268–275. ISSN: 17505836. DOI: 10.1016/j.ijggc.2015.07.014.

[65] Michael J. Wagner and Paul Gilman. *Technical Manual for the SAM Physical Trough Model*. Tech. rep. NREL/TP-5500-51825. Accessed: 2025-06-18. Golden, CO, USA: National Renewable Energy Laboratory (NREL), 2011.

[66] Junyao Wang et al. "Solar-Assisted CO2 capture with amina and amonia-based chemical absorbtion; A Comparative Study". In: *Thermal Science* 25 (1 Part B 2021), pp. 717–732. ISSN: 03549836. DOI: 10.2298/TSCI191222149W.

[67] Yongqiang Wang and Gang Kevin Li. "The impact of co-adsorbed water on energy consumption and CO2 productivity in direct air capture systems". In: *Separation and Purification Technology* 354 (2025), p. 129415. ISSN: 1383-5866. DOI: https://doi.org/10.1016/j.seppur.2024.129415.

[68] Peter Webb. *Scaling Direct Air Capture (DAC): A moonshot or the sky's the limit?* Oxford Institute for Energy Studies, 2023. ISBN: 9781784672232.

[69] Xiaowei Wu et al. "Technological Options for Direct Air Capture: A Comparative Process Engineering Review". In: *Annual Review of Chemical and Biomolecular Engineering* 18 (2024), p. 15. DOI: 10.1146/annurev-chembioeng.

[70] Chao Xu et al. "Energy and exergy analysis of solar power tower plants". In: *Applied Thermal Engineering* 31.17 (2011). SET 2010 Special Issue, pp. 3904–3913. ISSN: 1359-4311. DOI: https://doi.org/10.1016/j.applthermaleng.2011.07.038.

[71] John Young et al. "The impact of binary water–CO2 isotherm models on the optimal performance of sorbent-based direct air capture processes". In: *Energy Environ. Sci.* 14 (10 2021), pp. 5377–5394. DOI: 10.1039/D1EE01272J.

A

Faster adsorption model

In order to reduce the model to a pseudo-one-dimensional model, three different zones will be specified: a saturated zone with length x_{sat}, a mass transfer zone (MTZ) where the adsorption occurs with length l_{mtz}, and an unsaturated zone x_{unsat}, where the concentration will be the equilibrium concentration c_{out}. The adsorption in this zone will be 0. In every zone the average properties are being used. The three zones are schematically shown in Figure A.1. This figure is based on a constant effective reaction rate, based on the average concentration: $\bar{c}_{mt} = \frac{c_{in}+c_{out}}{2}$ and average sorbent loading: $\bar{q} = \frac{q_{eq}+q_0}{2}$ where q_0 is the initial sorbent loading and q_{eq} is the equilibrium sorbent loading, where $R_a = 0$.

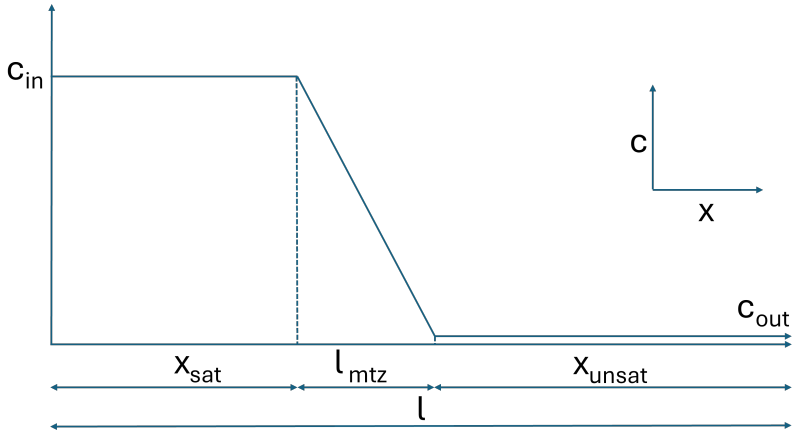

Figure A.1: Concentration profile over reactor length

To solve this system of ordinary differential equations, first the reaction rate has to be calculated with Equation 2.5. Subsequently, the Thiele modulus and effectiveness factor can be calculated to obtain the effective reaction rate ($R_{A,ef}$). This is the average sorbent loading over time, so it is one of the equations for which the system will be solved. With this value the length of the mass transfer zone (l_{mtz}) can be calculated. The mass balance over the MTZ can be rewritten, with $\frac{d\bar{c}_{mtz}}{dt} = 0$, to:

$$l_{mtz} = \frac{Q(c_{in} - c_{out})}{A(1-\epsilon_{void})\rho_s R_{A,ef}} \tag{A.1}$$

The mass transfer zone will move to the right due to the expanding saturated zone, which will continue to increase until it covers the entire column. Three derivatives are calculated to describe this situation:

$$\frac{d\bar{q}}{dt} = \bar{R}_{A,ef} \cdot \frac{l_{mtz}}{l} \tag{A.2}$$

$$\frac{dx_{sat}}{dt} = \frac{\bar{R}_{A,ef}}{q_{eq} - q_0} l_{mt} \tag{A.3}$$

$$\frac{dl_{mtz}}{dt} = 0 \tag{A.4}$$

A.1. Edge cases

The calculations with average values can only work properly, if the edge cases are accounted for as well. Especially for thin fixed beds used in adsorption, this becomes more relevant to obtain a valid model. Two edge cases can be defined, one at the inlet and one at the outlet. They both behave differently, so they will be discussed separately.

A.1.1. Inlet edge case

At the inlet, initially sorbent loading is equal to the initial sorbent loading everywhere in the MTZ. In the centre outside the edge cases, it has a constant profile. The MTZ will change in length at the inlet, as well as the concentration profile. There are a few methods to model this. The simplest model is to only start moving the saturated zone after a time (t_{dx}), that is required to load the mass transfer zone to the same profile as in the centre of the bed. This can be calculated by:

$$t_{dx} = \frac{\Delta q}{R_A} \tag{A.5}$$

Here it is assumed that R_A is constant, because it is limited by the ingoing concentration. It will have a smaller MTZ at first due to the low q at the start, but it will gradually increase until it has the same profile as in the centre. The value of q is the amount of sorbent loading needed to get to the desired profile:

$$\Delta q = q_{mtz} - q_0 = \frac{1}{2}(q_{max} + q_0) - q_0 = \frac{1}{2}(q_{max} - q_0) \tag{A.6}$$

Where q_{max} is the maximum sorbent loading that can be obtained, at a pressure and temperature, by setting $R_A = 0$ in Equation 2.5. With solely this formula, $\frac{d\bar{c}}{dt}$ is neglected, which is largest at the initial time. This method is valid when at the start: $lmtz < l$,

The method described above only works when: $l_{mtz} < l$, where l is the length of the bed. When this is not the case, the rate of the CO_2 adsorption will already start to decrease, since the whole concentration will not be adsorbed within this mass transfer length. The method to solve this is discussed in Appendix A, this is not implemented in the end because the model without averages is already really fast compared to the desorption model.

A.1.2. Outlet edge case

In the outlet edge case the following situation arrises at the end: $x_{sat} + l_{mt} < l$ and the MTZ effectively becomes:

$$l_{mt,ef} = l - x_{sat} \tag{A.7}$$

This can not be negative, when a negative number comes from this calculation, it will be changed to 0. With the MTZ now being smaller than necessary to adsorb all CO_2, the total adsorption will decrease. The effective value of $R_{A,ef}$ is now:

$$R_{A,ef} = \eta_{ads} R_A \frac{l_{mt,ef}}{l_{mt}} \tag{A.8}$$

With this new value of $R_{A,ef}$, $\frac{d\bar{q}}{dt}$ and $\frac{dx}{dt}$ can be calculated with formulas A.2 and A.3. The last formula becomes:

$$\frac{dl_{mt}}{dt} = -\frac{dx}{dt} \tag{A.9}$$

A.1.3. Validate average assumption

To determine if the assumption is valid that the mass transfer profile can be defined by taking the average concentration and sorbent loading, the real profile of c and q must be calculated once. This can be done by rewriting the mass transfer balances to obtain $\frac{\delta c}{\delta t}$ and $\frac{dq}{dt}$.

The solid mass balance already gives the relation for $\frac{\delta q}{\delta t}$ in Equation 2.5. The mass balance for the gas phase is given in 2.15, which can be rewritten for very small slabs of width Δx, to:

$$A\epsilon_{void}\Delta x\frac{\delta c}{\delta t} = Av_s(c_{in} - c_{out}) - R_A A(1-\epsilon_{void})\Delta x \tag{A.10}$$

Which gives the partial derivative:

$$\frac{\delta c}{\delta t} = -\frac{v_s}{\epsilon_v}\frac{\delta c}{\delta x} - R_{A,ef}\frac{1-\epsilon_v}{\epsilon_v}\rho_s \tag{A.11}$$

These two equations can be solved with the method of lines. The length of the bed will be subdivided into smaller segments, where the concentration and sorbent loading will be calculated by the first-order upwind scheme, based on the previous values. This method represents the advection, since the concentration and sorbent loading are merely dependent on the upwind values as well. The diffusion is only added in the efficiency, and is not being calculated different numerically. This scheme looks like:

$$\frac{\delta c}{\delta x} = \frac{c(x) - c(x-\Delta x)}{\delta x} \tag{A.12}$$

The stability of the system can be checked by the Courant-Friederichs-Lewy condition. This stability criterion for explicit numerical integration is:

$$\frac{v_s\Delta t}{\Delta x} \leq 1 \tag{A.13}$$

This model can be used to create the benchmark model, which can be compared to the simplified models. The change over time is shown in Figure A.2.

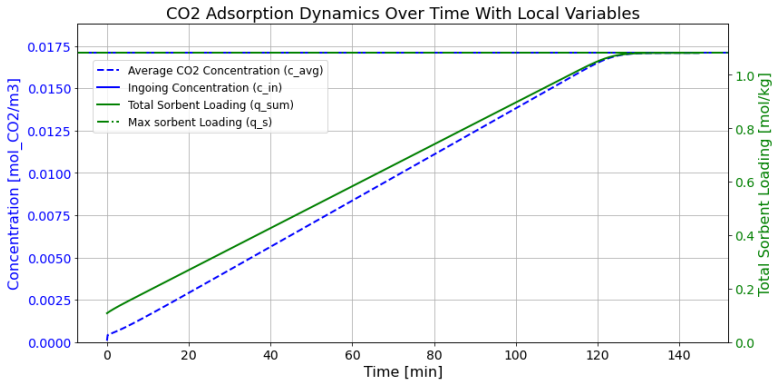

Figure A.2: Concentration and sorbent loading based on method of lines

A.1.4. Model limits

With the breakthrough curve obtained from Schellevis et al. in Figure A.6, it becomes clear that there are limits to the simplified model. In this case the mass transfer zone that is required, is almost instantly larger than the column length. This creates large issues with the assumption of the shape of the profile. The real shape of the profiles can be seen in Figure A.3.

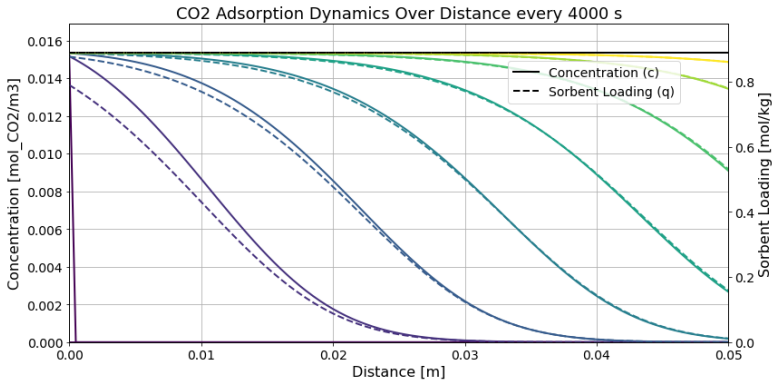

Figure A.3: Shape of curve

A.2. Faster desorption improvement

In order to account for the problems faced at adsorption where at the start $l_{mtz} < l$ holds, a method is taught of which could not be implemented due to the small gain it gives for this research. This method still makes the assumption that the average profile looks like a straight declining line, the profiles will change over time as displayed in Figure A.4.

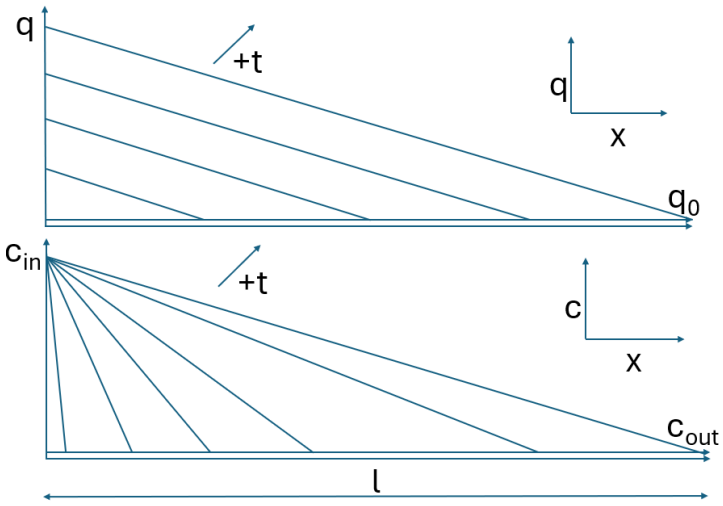

Figure A.4: Schematic of the profiles of q and c at the beginning

The value of q at $x = 0$ will increase until it reaches q_{max} with:

$$\frac{dq}{dt} = R_a \frac{l_{mt}}{l} \tag{A.14}$$

At the same time l_{mt} is increasing with:

$$\frac{dl_{mt}}{dt} = \frac{R_a}{q} \rho_s (1 - \varepsilon_{void}) \tag{A.15}$$

When the desired q_{max} is reached, the saturated zone starts to increase:

$$\frac{dx}{dt} = \frac{R_a}{q_{sol} - q_0} l_{mt} \tag{A.16}$$

A.2.1. Verification

The first breakthrough curve is correct for both the average and regular model and the second one is only correct with the regular model, because it has a small length compared to the mass transfer zone.

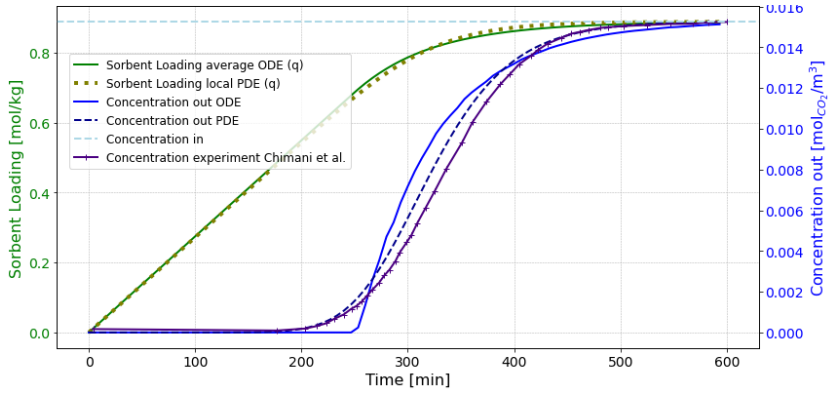

Figure A.5: Breakthrough curve validation with data from Chimani et al. [15]

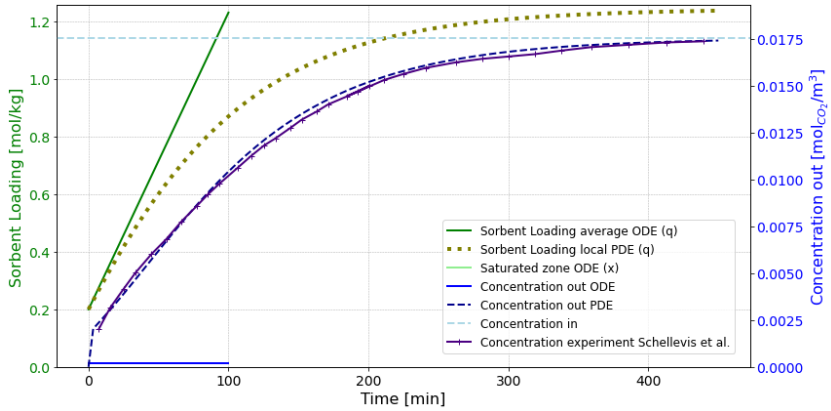

Figure A.6: Breakthrough curve validation with data from Schellevis et al. [54]